May 2017

Plug-In Grid Compatible Next Generation Power Converters

Qianqian Jiao
University of Wisconsin-Milwaukee

PLUG-IN GRID COMPATIBLE NEXT GENERATION POWER CONVERTERS

by

Qianqian Jiao

A Thesis Submitted in

Partial Fulfillment of the

Requirements for the Degree of

Master of Science

in Engineering

at

The University of Wisconsin-Milwaukee

May 2017

ABSTRACT

PLUG-IN GRID COMPATIBLE NEXT GENERATION POWER CONVERTERS

by

Qianqian Jiao

The University of Wisconsin-Milwaukee, 2017
Under the Supervision of Professor Robert M. Cuzner

The utilization of the DC low voltage distribution opens new possibilities for network development. Community DC microgrid is considered as an efficient solution for providing clean energy for residential areas. The connection of the DC microgrid to the AC utility grid would need a power electronic based rectifier. Voltage Source Rectifier (VSR) and Current Source Rectifier (CSR) are considered as the two options for such application. This study compares the two topologies based on their power density and efficiency. Silicon Carbide (SiC) switches are used for designing the rectifiers to get better power density and efficiency. The proximity of the rectifier to the residential area requires electromagnetic compatibility (EMC) of the rectifier with established standards such as IEC 61000-3-4 and FCC B. This analysis shows that CSR has higher efficiency and higher power density compared to VSR.

TABLE OF CONTENTS

LIST OF FIGURES

LIST OF TABLES

ACKNOWLEDGEMENTS

Even though a master thesis is an independent work, it would not have been possible without the support of many people.

First, I would like to express my gratitude to my advisor Professor Robert M. Cuzner for his support during my Master study. His guidance and encouragement inspired me a lot during my research.

I would like to thank my committee members, Dr. Nasiri and Dr. Fu.

I would like to thank my friends and former colleague, Jiangbiao He, Xu Yang, Yujia Cui, Hui Xie, Xiaolu Yin, Limu Ke, Yali Liu, who gave me great help.

Last but not the least, I sincerely thank my family for all their support and love, this work would not be possible without you.

1 INTRODUCTION

A community DC microgrid is proposed as a feasible solution for providing residential DC power distribution in urban neighborhoods [1]. Such a DC microgrid would supply renewable and environmentally friendly electricity to a group of consumers located in a neighborhood or proximity to each other. The DC microgrid would facilitate the consumers with the utilization of renewable energy resources such as solar energy and independent energy resources like combined heat and power (CHP). The nominal DC bus voltage is 350Vdc. This research has informed the author's perspective on a community DC microgrid as an economical solution for the community either as the main infrastructure for the electricity or as a backup for emergency situations. Figure 1-1 shows the schematics of the proposed architecture of the community DC microgrid.

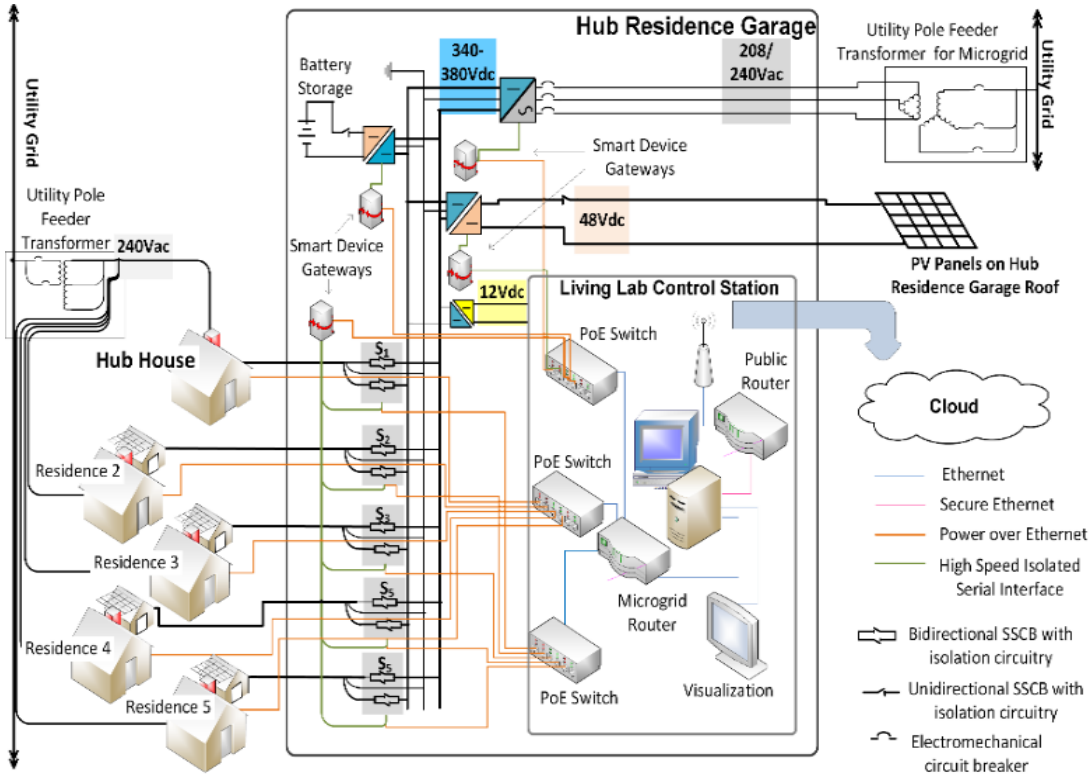

Figure 1-1 Architecture of the proposed Community DC microgrid

As illustrated in Figure 1-1, the proposed topology for such a DC microgrid designates one of the houses as a hub house. The hub house is the center for control and conversion of energy. The connection between the DC microgrid and the AC grid would take place in the garage of this house. A conversion of the AC power to the DC power eventuates using a three-phase rectifier. There are two established options for the development of such a rectifier: Voltage Source Rectifier (VSR) and Current Source Rectifier (CSR).

In this thesis, a comparison between VSR and CSR are presented with attention to filtration required for meeting the EMI limits for the rectifiers to be used in community DC microgrid. This study will determine which of the two options of VSR and CSR is more suitable for such application assuming a 30kVA input feed system rating. Efficiency and energy density are the main factors that will be considered for this analysis. The rest of this paper are organized as follow: Chapter 2 introduces DC microgrid, the topologies and specifications of the two converters, and the EMC consideration. Chapter 3 presents filter design methodology combined with discussions. The procedure of designing both differential mode (DM) and common mode (CM) filters are explained in this section. Chapter 4 presents the results of the analysis and comparison between the two topologies. Chapter 5 presents the PWM methods of VSR and CSR. Chapter 6 explores the simulation model and results. Chapter 7 shows the experimental setup and Chapter 8 concludes the work.

2 STATE OF THE ART

The main contribution of this research is the design of the most power dense and efficient rectifiers. In order to express this research properly, this chapter provides a review of the DC microgrid, the power rectifiers, the SiC devices, and the EMC consideration.

2.1 Community DC Microgrid

Generally speaking, a microgrid is a discrete energy system consisting of distributed energy sources (including demand management, storage, and generation) and loads capable of operating in parallel with, or independently from, the main power grid. The primary purpose is to ensure local, reliable, and affordable energy security for urban and rural communities, while also providing solutions for commercial, industrial, and federal government consumers. In many respects, compared with the traditional power grid, microgrids are the small-scale versions. The Department of Energy (DOE) defines the microgrid as "A group of interconnected loads and distributed energy resources (DERs) with clearly defined electrical boundaries that acts as a single controllable entity with respect to the grid and can connect and disconnect from the grid to enable it to operate in both grid-connected or island mode [2]." Under these definitions, the community DC electrical system itself is categorized as a microgrid.

2.2 AC to DC Power Converters

AC to DC power converters have a wide application, including the adjustable-speed drives (ASDs), switch-mode power supplies (SMPSs), uninterrupted power supplies (UPSs), battery charging for electric vehicles, DC microgrid and so on [3]. The ac–dc converters are called rectifiers; they

convert the AC power to DC power by using diodes and controlled switches. According to the source supply, the rectifiers are divided into voltage source rectifiers and current source rectifiers.

2.2.1 Voltage Source Rectifiers

The VSR is the most widely used active rectifier and operates by maintaining the DC link voltage at the desired value using feedback control. VSR can also be called a voltage boost rectifier because its DC output voltage is typically higher than the peak of the line input voltage. Depending on the application, this characteristic of the VSR could be an advantage or a disadvantage. If the required DC voltage is greater than the peak of the input AC voltage, the VSR is a good choice, and if the required DC voltage is lower than the peak input AC voltage, then VSR is not the best choice because additional bucking circuitry would be required. This may be a concern when it comes to mitigating fault behavior in the DC microgrid because the VSR cannot provide a current limit on its output. The system will rely completely upon upstream AC circuit breakers or downstream DC solid state circuit breakers for protection with the VSR. The capability of bi-directional power flow is also one of the benefits of VSR.

In this work we utilize the design of the VSR utilizing the Silicon Carbide (SiC) based MOSFET with SiC Junction Barrier Schottkey (JBS) diodes. The 1200V, 100A, SiC Half-Bridge Module fabricated by Cree [4] is used for the VSR. The SiC MOSFET/Diode can operate at higher voltage, higher temperature and higher switching frequency than its Silicon IGBT counterpart, and thus higher power density is achieved. Pulse width modulation (PWM) generates logic for the gate signals feeding the SiC devices. Figure 2-1 shows the topology of a three phase VSR.

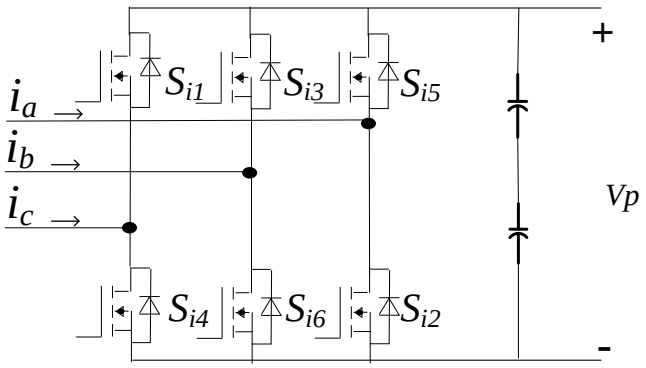

Figure 2-1 Voltage Source Rectifier

2.2.2 Current Source Rectifiers

The CSR or buck rectifier also operates based on PWM switching and closed loop control. If the required DC voltage is lower than the peak of the input AC voltage, the CSR is a good choice. For the DC microgrid, the CSR also has the added benefit of being able to current limit its output in the presence of a fault [5]. This may be an advantage for the DC microgrid because it provides additional flexibility for fault management where the upstream converter can coordinate with downstream solid state circuit breakers, and all DC microgrid fault behavior is completely isolated from the upstream AC feed. Note that the consideration of input AC voltage peak voltage to DC output voltage ratio and whether or not a VSR or CSR is the best choice is not a significant consideration because a feed transformer between the utility and the input of the AC to DC converter will be required. A VSR will require a three phase 208V secondary on that transformer while the CSR would require a three phase 480V secondary.

Recent studies show the possibility of getting higher power density and lower conducted electromagnetic interference (EMI) using CSRs for power ranges below 20 kW using Silicon Carbide (SiC) switches with the diodes in series [6]. In this study, the rating power of the CSR is

considered 30 kW. Figure 2-2 shows the topology of CSR. Proper filters are required to be added to both VSR and CSR to mitigate the harmonics and the EMI that will be generated as a result of fast switching of the SiC switches [7], [8].

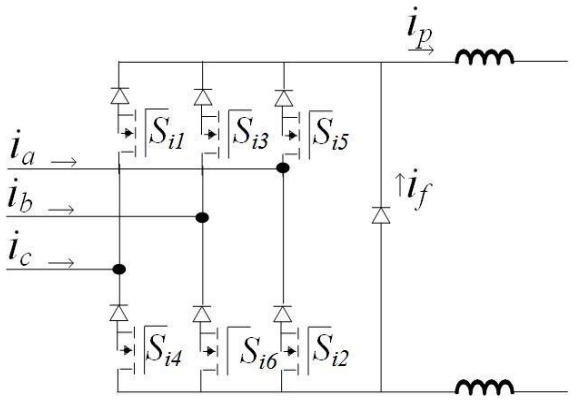

Figure 2-2 Current Source Rectifier

2.3 Silicon Carbide (SiC) power devices

Silicon (Si) based devices is by far the most widely used power semiconductor devices. While with the rapid developments in the industry and other power area, more and more issues occur and the semiconductor industry is urged to find higher performance devices, which has higher breakdown voltage, higher operating electric field, higher operating temperature, higher switching frequency, and lower losses. Due to the inherent material limitation of Si-based power devices, Silicon Carbide (SiC) power devices are innovated and developed, which meets all these demands.

Compared with silicon-based devices, the SiC devices have higher blocking voltages, lower on-state resistance and switching losses, higher operating switching frequency, higher thermal conductivity and operating temperatures. Therefore, using SiC-based devices has the significant advantages of reduced thermal management requirements, smaller passive components, fewer

filter losses, which result in higher system efficiency and higher power density. Even though the SiC devices are still in the early stage and their price is higher than Si devices, considering all the compelling advantages of SiC devices, its benefit will be significant enough to offset the higher cost. The SiC-based devices have some significant advantages over the Si-based devices; this is due to some of the favorable characteristics of SiC. First, it has a higher critical electrical field, which leads to lower losses. Second, SiC has much higher thermal conductivity, therefore lower temperature drop. Third, it has a higher melting temperature. Hence it can operate at higher temperature, which is over 400°C. And also, SiC has higher current density. Therefore the devices will reduce the cost.

Right now, the commercially available SiC power devices are MOSFETs, Schottky diodes, JFETs and BJTs, and it has become a crucial part for next generation power converters. In this thesis, considering the parameters of the system, CAS120M12BM2 is selected as the switching device, the product photo and the schematic are shown in Figure 2-3 and Figure 2-4.

Figure 2-3 Silicon Carbide, Half-Bridge Module CAS120M12BM2

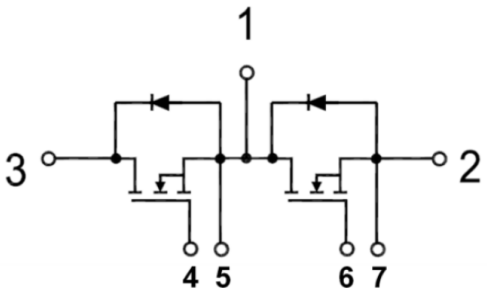

Figure 2-4 Schematic of Silicon Carbide, Half-Bridge Module CAS120M12BM2

2.4 EMC Consideration

The wide band gap switching device operates at ten times higher switching frequency than the Si-based device, which making possible more compact, less costly product designs. While the high frequency effects bring more challenges, such as the RF and microwave electronics as shown in the figure below. In this study, only the frequency range below 30MHz is considered.

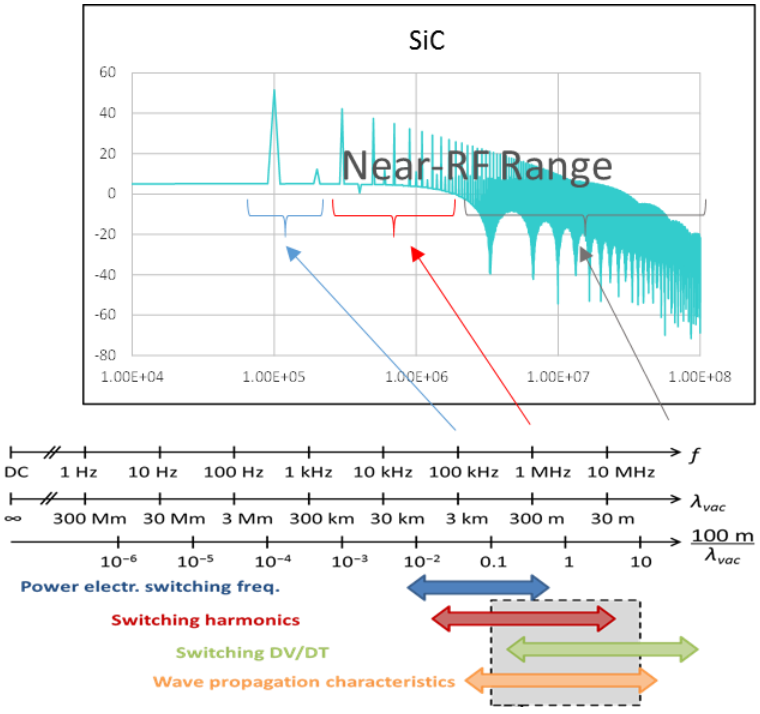

Figure 2-5 SiC high frequency challenge

Electromagnetic compatibility (EMC) is concerned with the unintentional generation, propagation and reception of electromagnetic energy which may cause unwanted effects such as electromagnetic interference (EMI) or even physical damage to operational equipment.

There are two main classes of issues for EMC as shown in Figure 2-6. The first one is emission, which is the generation of electromagnetic energy by some source and its release into the environment, no matter it is deliberate or accidental. The second one is susceptibility, which is the tendency of electrical equipment, referred to as the victim, to malfunction or break down in the presence of unwanted emissions, which are Radio frequency interference.

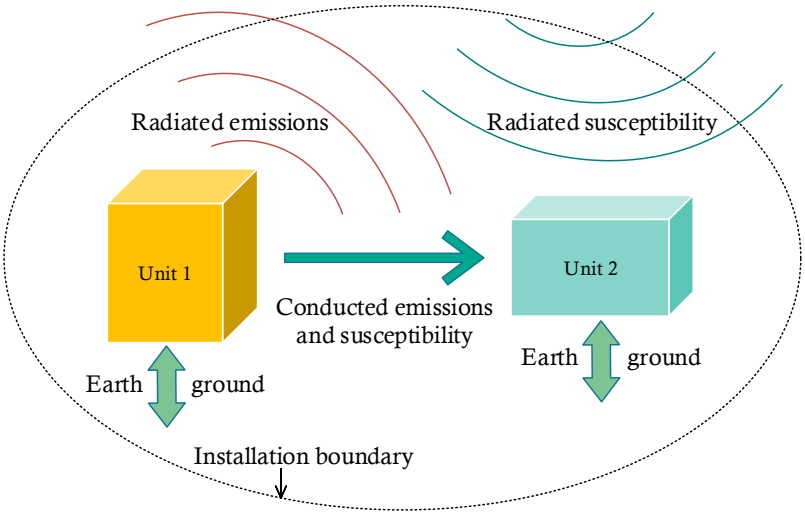

Figure 2-6 Emissions and Susceptibility

EMC studies the unwanted emissions and the countermeasures to reduce the unwanted emissions. And the emissions are divided into two groups, conducted electromagnetic emissions and radiated electromagnetic emissions. The EMC environment is shown in Figure 2-7. In this thesis, only the conducted electromagnetic emissions are taken into consideration.

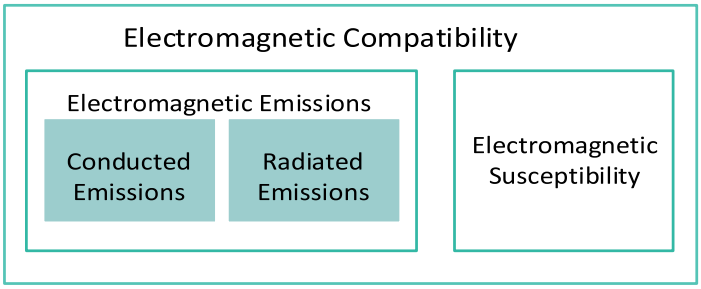

Figure 2-7 EMC environment

2.4.1 EMC at High Frequency

In the USA, in order to prevent interference to radio and TV broadcast reception, and to other sensitive services, the electromagnetic emissions are regulated by the Federal Communications Commission (FCC). The industrial emissions from RF and digital devices are regulated under FCC Part 15, Subpart B, Class A limits. In this thesis, the converters are used in residential areas, community microgrids must meet the regulation under FCC Part 15, Subpart B, Class B limits. Table 1summarizes the EMC standards for various environments in the USA. Note that the residential environment is the one concerned in this thesis. Figure 2-8 and Table 2 shows the details of FCC Part 15 Class B emission limits.

Table 1 EMC standard in the USA

Environment	USA-FCC
	emissions only
residential	Part 15 Class B
commercial	Part 15 Class A
light industrial	
industrial	
public utility or industrial plant	No interference

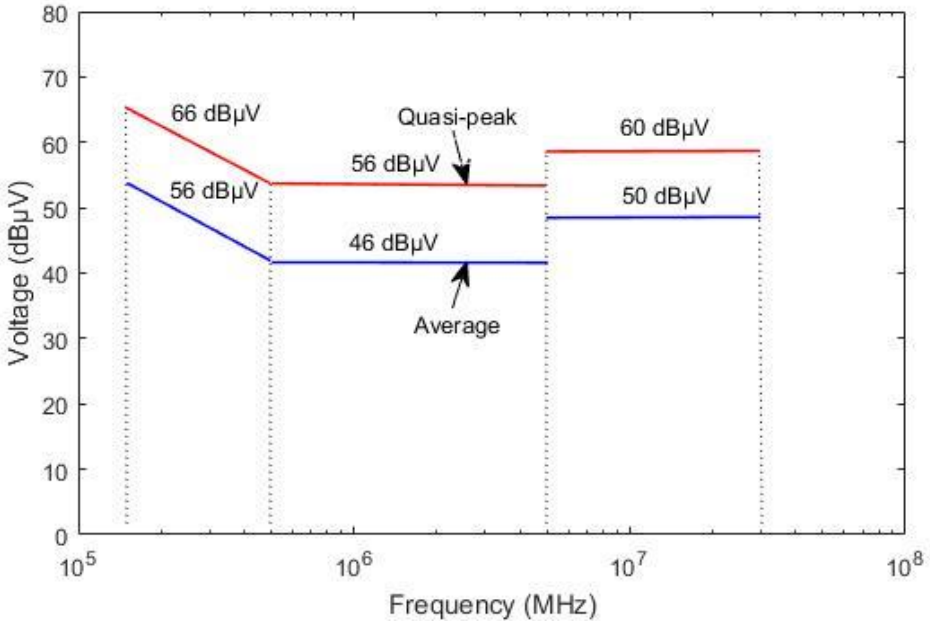

Figure 2-8 FCC/CISPR limit for conducted emission for Class B digital devices

Table 2 FCC Part 15/CISPR 22 Conducted Emission limit (class B)

Frequency (MHz)	Quasi-Peak		Average	
	μV	dBμV	μV	dBμV
0.15-0.5	1995-631	66.0-56.0	631-199.5	56.0-46.0
0.5-5	631	56	199.5	46
5-30	1000	60	316	50

For a device with conduct noise current, when it is connected to the power network, the noise currents would flow out of the device and onto the power network and finally affect the overall power grid. On one hand, this noise can flow onto other devices connected to the power network through the wire, on the other hand, the electrical length of the conductors that comprise the power network may generate radiation due to this noise. In order to impose conducted emissions standards on products to reduce the overall noise level on a given power network, the device Line Impedance Stabilization Network (LISN), is used to measure the conducted emissions. As shown in Figure 2-9, the LISN is inserted in series with the power cord of the Device Under Test (DUT).

In the USA, the conductors for AC system are divided into three classes, the phase (P) conductors, neutral (N) conductors and Green Wire (GW). The GW is the conductor which is safely grounded. And the LISN measures the noise currents which exists in the phase and neutral conductors.

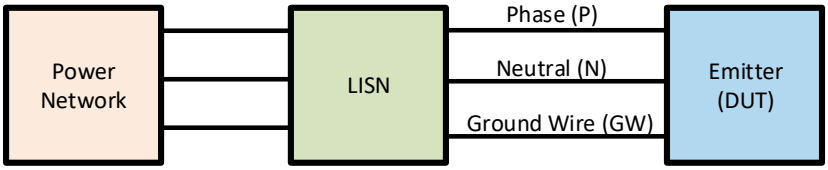

Figure 2-9 Conduction emission test schematics

Figure 2-10 shows the schematics of a one phase LISN that is used to measure the conducted emissions. From the schematics, it is obvious to find that the inductor L acts as an RF choke, and the capacitor C near the power network acts as an RF shunt. At low frequency, the impedance of inductor is very low, which is essentially a short circuit, and the impedance of capacitor is very high, which is essentially an open circuit. Therefore, this combination of L and C can block the high-frequency noise from the power network while allowing the low fundamental frequency power signal to pass through. Since this structure blocks the noise currents from the power network and can prevent it from contaminating the test results, LISN could have a more accurate measurement of the DUT noise currents.

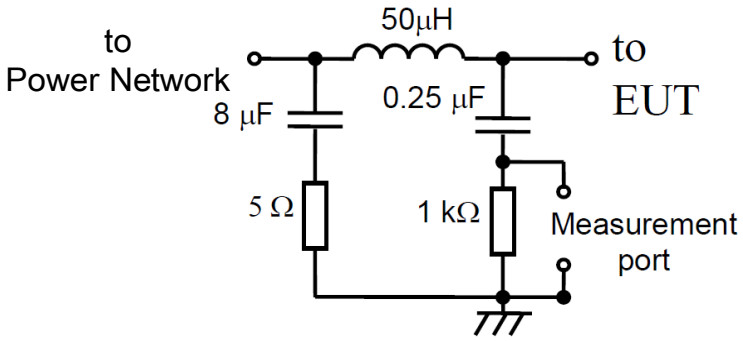

Figure 2-10 LISN for one phase measurement

2.4.2 EMC at Low frequency

The standards regulating EMC at high frequency has been discussed in the previous section, while there are some other standards must be meet for EMC at low frequency. And this section gives more details about the EMC at low frequency.

Table 3 EMC low frequency standards

Standards	IEC 61000-3-2	IEC 61000-3-4
Goal	Limits for harmonic current emissions (equipment input current less than 16A per phase)	Limitation of emission of harmonic currents in low-voltage power supply systems for equipment with rated current greater than 16 A per phase

From Table 3, there are two main differences between IEC 61000-3-2 and IEC 61000-3-4. One is the voltage range, IEC 61000-3-4 only applies to low-voltage power supply systems, another is the rated current, system with current greater than 16 A must meet the IEC 61000-3-4 standards.

Table 4 IEC Standard Voltages

IEC voltage range	AC (Vrms)
High voltage (supply system)	> 1000
Low voltage (supply system)	50–1000
Extra-low voltage (supply system)	< 50

Table 5 VSR and CSR AC side operating scenario parameters

Parameter	Name	VSR	CSR	Unit
Rated Power	Prated	30	30	kVA
Input Voltage	Vllrms	208	480	V
Input Current	Irms	83.3	36.1	A

Table 4 gives the standard voltage classifications. And Table 5 lists the parameters of the system operating scenario. The input voltage of VSR and CSR are 208 V and 480 V correspondingly,

which is in the range of [50 V, 1000 V]. Therefore, the systems belong to the low voltage supply. Also, the input current of VSR and CSR are 83.3 A and 36.1 A correspondingly, which are greater than 16 A. Hence, for EMC at low frequency, the system of this thesis must satisfy the IEC 61000-3-4 standards, which is shown below:

Table 6 IEC 61000-3-4 standards

Harmonic number	3	5	7	9	11	13	15	17	19
Admissible IHD %	21.6	10.7	7.2	3.8	3.1	2	0.7	1.2	1.1
Harmonic number	21	23	25	27	29	31	33	Even	
Admissible IHD %	0.6	0.9	0.8	0.6	0.7	0.7	0.6	$\leq 8/n$ or ≤ 0.6	

3 Filter Design

The filters take a lot of space compared with other components in the system, and also result in a big portion of the energy loss. In order to design the most power dense rectifiers, the filter design part is a main work in this thesis. Filters are normally composed of inductors and capacitors. Since capacitors can not be customized, they are provided with certain characteristics; the size is given once the capacitance is determined. Therefore, the design mainly focuses on the inductor characteristics. And the first section gives a detailed design process for inductor design.

3.1 Inductor Design

This section discusses the inductor design. To goal is to find the inductor which has the minimum volume. There are different types of inductor, including air core inductor, iron core inductor, ferromagnetic core inductor, toroidal inductor, and so on. In this thesis, the filter is designed for the system whose switching frequency is 40 kHz. By searching the different types inductors and comparing the characteristics, metglas amorphous alloys are found to have very low loss and can operate at high frequency, so they are selected as the core material for the differential mode and common mode inductor design. Figure 3-1 shows the equivalent circuit of an inductor with an air gap. The air gap is required for preventing the saturation of the core and keep the inductance as a constant.

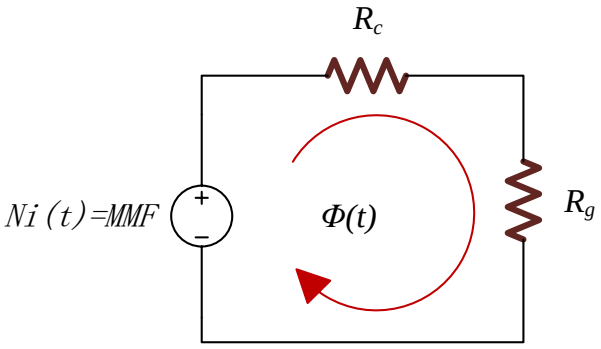

Figure 3-1 Equivalent circuit of an inductor with air gap

In Figure 3-1, *N* is the turns of the coil, *i(t)* is the current in the coil, *Ni(t) is* the magnetomotive force, R_c is the reluctance of the core, R_g is the reluctance of the air gap. The magnetic equation is:

$$NI = \Phi R_g + \Phi R_c \tag{3-1}$$

The reluctance of air and core is expressed as:

$$R_g = \frac{l_g}{\mu_0 A_c F_r} \tag{3-2}$$

$$R_c = \frac{l_c}{\mu_c A_c} \tag{3-3}$$

In Equation 3-2 and 3-3, F_r is 1.05, μ_0 is $1.26\times10{-}6$ $H\cdot m^{-1}$, while the μ_c is around 50000 for metglas, so R_g is much larger than R_c, which can be neglected. Hence,

$$NI_{peak} \approx \Phi R_g = B_{max} A_c \frac{l_g}{\mu_0 A_c F_r} = \frac{B_{max} l_g}{\mu_0} \tag{3-4}$$

And the relation between inductance and turns number is expressed by the following:

$$L_{dm} = \frac{N^2}{R_g} = \mathrm{N}\frac{N}{R_g} = N\frac{\Phi}{I_{peak}} = \frac{\mathrm{N}B_{max}A_c}{I_{peak}} \tag{3-5}$$

Also, we have the equation:

$$A_w = \frac{I_{rms}}{J} \tag{3-6}$$

A_w is the conduction area of the conductor, J is the maximum current density, which is 4.96 e^6 A/m^2. With the A_w give, the window area WA can be obtained by the following:

$$WA = \frac{N \times A_w}{K_u} \tag{3-7}$$

K_u is the fill factor, which is 0.4. By solving the equations from 3-4 to 3-7, then A_c and WA can be obtained.

To get the minimized volume, the inductor is assumed to be a cube. Figure 3-2 gives the outline of a metglas core inductor.

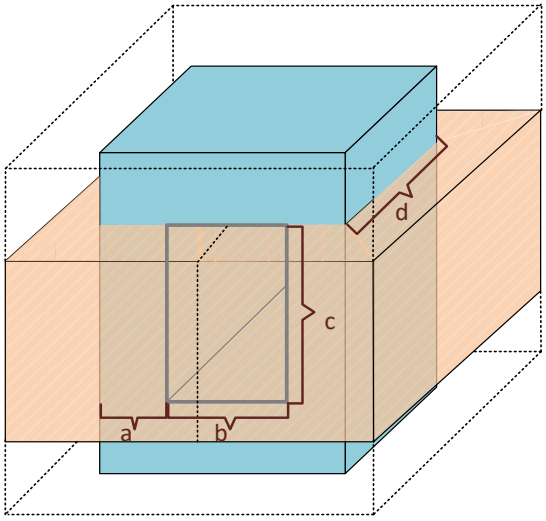

Figure 3-2 Outline of an inductor with core

Figure 3-2, the equations can be expressed as:

$$A_c = a \times d \tag{3-8}$$

$$WA = b \times c \tag{3-9}$$

$$Volume = (c + 2a)^3 \tag{3-10}$$

With the constraint of the cube, the corresponding equations are expressed in the following:

$$2a + 2b = d + b \tag{3-11}$$

$$d + b = c + 2a \tag{3-12}$$

By solving the Equations 3-8 through 3-12, the size of the inductor can be calculated.

The above part exactly applies to the differential mode inductor design in this thesis. While the common mode inductor is designed in scale and proportion principles. In general, the size, inductance, and current of an inductor have the following relationship:

$$Volume \propto L \times I_{rms,cu} \times I_{pk,core} \tag{3-13}$$

For DM inductor and CM inductor, $I_{rms,cu}$ is the same, which is the rated current. But the $I_{pk,core}$ is different, it is the peak value of the copper current for DM inductor, and it is the peak value of the ground current for CM inductor. Since the CM current is much smaller than DM current, the CM inductor size is also proportionally smaller than DM inductor. CM inductor has larger window area, since there are three windings compared with DM inductor which only has one winding. While considering that there is only one CM inductor needed while there are three DM inductor required for the circuit, the total volume of CM inductors is still much smaller than that of the DM inductors.

3.2 Design process

This section provides a detailed description of the two converter topologies with the specifications used for designing the converters in this study for further analysis. The connection to the grid

imposes limitations for designing the power electronics converters. DM and CM noises are defined in following equations:

$$V_{a\_dm} = V_{ag} - V_{cm} \tag{3-14}$$

$$V_{cm} = \frac{V_{ag} + V_{bg} + V_{cg}}{3} \tag{3-15}$$

and V_{ag} is the phase voltages compared to the ground, V_{a_dm} is the DM noise of phase "a" and V_{cm} is the common mode voltage.

The DM and CM filters are designed to meet a specified EMI requirement as measured at a line to ground connected LISN when the system is excited by the DM and CM components of voltage produced by the rectifiers. To maximize the power density, the design will achieve a minimum volume. This power density limitation is a result of the inductor design. In the high-frequency range, inductor design and core material selection play an important role, and more work needs to be done to improve it.

The methodology of a filter designed is explained in detail in refs. [9], [10] and [11]. The measured voltage across the LISN's resistor of the original circuits without any filter is expressed in dBμV, then compared with the EMI standards requirement and consequently, the frequency-dependent attenuation value is obtained. The filters should be designed in a way that the calculated frequency dependent attenuation is obtained. The designed filters must meet IEC 61000-3-4 standard for frequencies smaller than 0.15 MHz and for frequencies higher than 0.15 MHz, the conducted emission has to meet FCC B. Table 1 shows the values corresponding to the standards used for filter design in this work. In the following, the procedure of filter design is explained in more detail.

Table 7 Standards used for filter design

IEC 61000-3-4									
Harmonic number	3	5	7	9	11	13	15	17	19
Admissible IHD %	21.6	10.7	7.2	3.8	3.1	2	0.7	1.2	1.1
Harmonic number	21	23	25	27	29	31	33	Even	
Admissible IHD %	0.6	0.9	0.8	0.6	0.7	0.7	0.6	≤8/n or≤0.6	
FCC B									
Frequency (MHz)	0.15-0.5			0.5-5			5-30		
Peak (dBμV)	66-56			56			60		

3.2.1 DM EMI Filter Design

To design filters for the three phase rectifiers, there are five steps.

1. Create the DM equivalent circuit for the original rectifiers, which has no DM filters. Derive its transfer function.
2. Add DM filter to the circuit, and assume the relationships among the components. Create its equivalent DM circuit and derive the transfer function.
3. Measure the FFT at a specific frequency, compare it with the standards limitation, and using the transfer function from step 1 and step 2 to get a function of L and C.
4. Using the relation between the volume and the parameter value of the filter to get the second function of L and C.
5. Solve the functions from step 3 and step 4 to get the value of L and C for the filter.

The following part gives the detailed design process step by step.

Step 1: Given the original three-phase VSR and CSR as shown in Figure 3-3 and Figure 3-4, then the one phase DM equivalent circuit can be obtained as shown in Figure 3-5 and Figure 3-6.

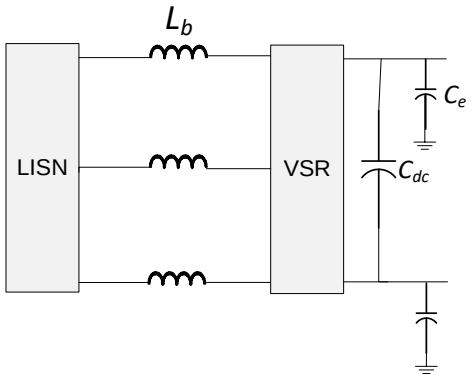

Figure 3-3 VSR without filter

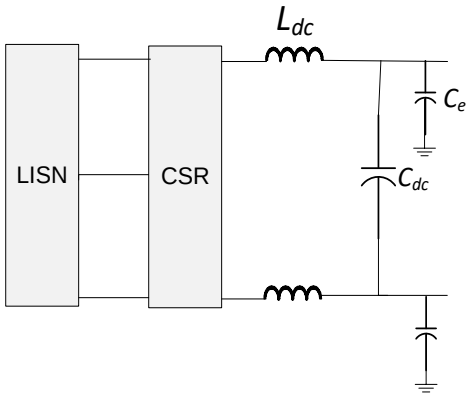

Figure 3-4 CSR without filter

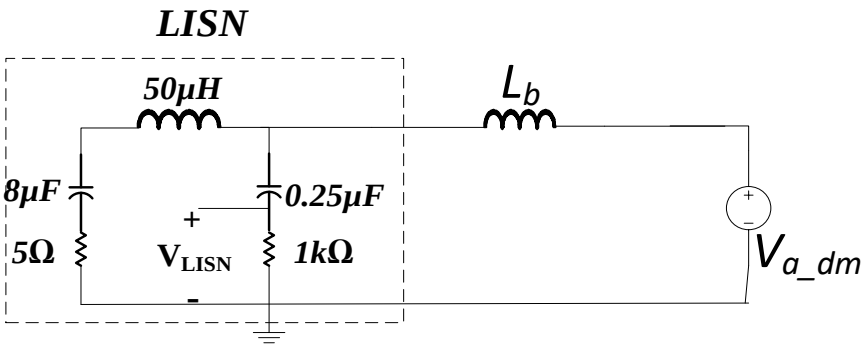

Figure 3-5 DM equivalent circuit for VSR without filter

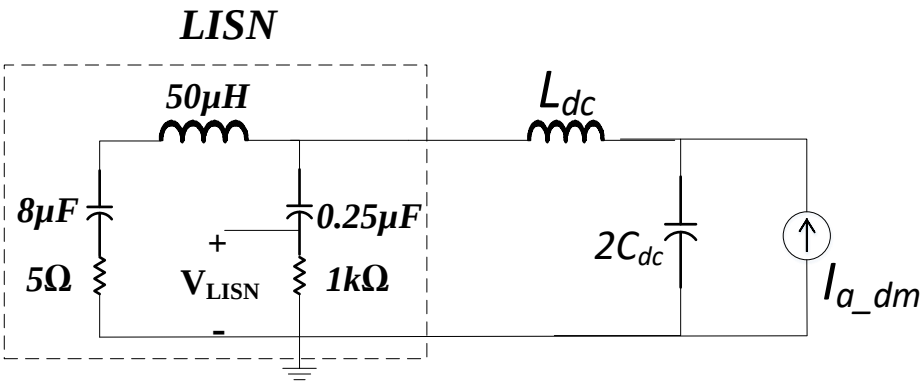

Figure 3-6 CM equivalent circuit for VSR without filter

With the equivalent circuit, the transfer function for VSR and CSR without filter are obtained in following equations:

$$\left|\mathrm{TF}_{VSR\_o}\right| = \left|\frac{I_{LISN}}{V_{o\_dm}}\right| = \left|\frac{1}{sL_b}\right| \tag{3-16}$$

$$\left|\mathrm{TF}_{VSR\_o}\right| = \left|\frac{I_{LISN}}{V_{o\_dm}}\right| = \left|\frac{1}{sL_b}\right| \tag{3-17}$$

Step 2: Based on the properties of the circuits, the LCL filter is selected as the DM filter For VSR, and the LCLC filter is selected for CSR. The most inboard DM inductors are the largest in order to filter the EMI noise. L_{dm2} performs the most attenuation. The inductors are selected as $L_{dm2} = 3\ L_{dm1}$ for VSR and $L_{dm2} = 20\ L_{dm1}$ for CSR. Then the new circuit and its DM equivalent circuit are given in following figures:

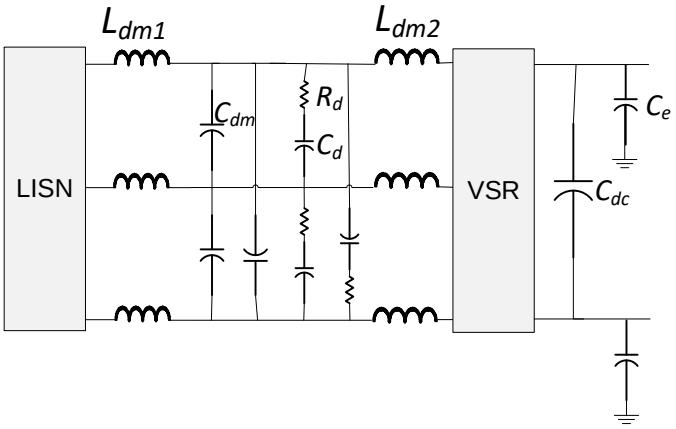

Figure 3-7 VSR with DM filter

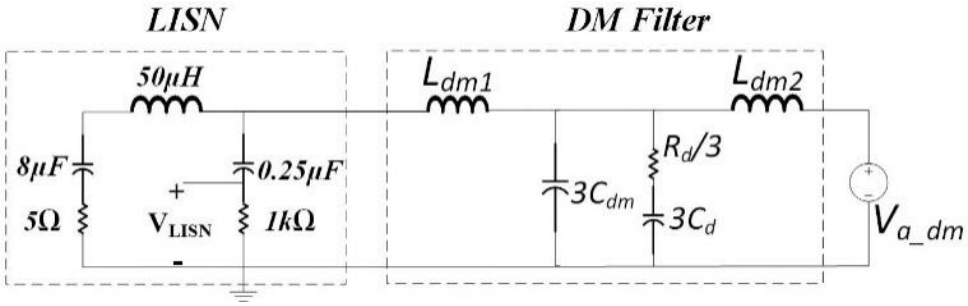

Figure 3-8 DM equivalent circuit for VSR with DM filter

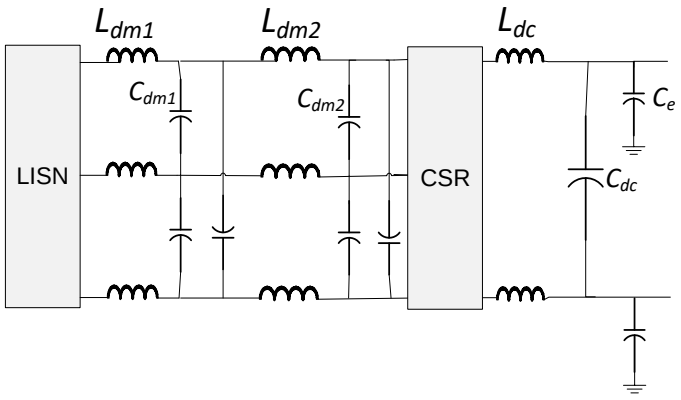

Figure 3-9 CSR with DM filter

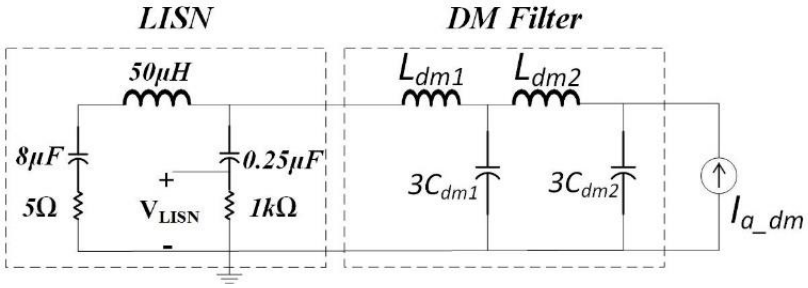

Figure 3-10 DM equivalent circuit for CSR with DM filter

The transfer functions of the DM filter are expressed in following equitation:

$$\left|\mathrm{TF}_{VSR\_DM}\right| = \left|\frac{I_{LISN}}{V_{a\_dm}}\right| = \left|\frac{1}{s^3 3C_d L_{dm1} L_{dm2} + s(L_{dm1}+L_{dm2})}\right| \tag{3-18}$$

$$\left|\mathrm{TF}_{CSR\_DM}\right| = \left|\frac{I_{LISN}}{I_{a\_dm}}\right| = \left|\frac{1}{s^4 C_{dm1} C_{dm2} L_{dm1} L_{dm2} + s^2 (L_{dm1}+L_{dm2})(C_{dm1}+C_{dm2})+1}\right| \tag{3-19}$$

Step 3: Run the simulation model of VSR and CSR without a filter, measure the DM current through LISN, carry out the Fast Fourier Transform (FFT) of the current by using the Fourier spectrum function of the PLECS. Find the absolute FFT value of the current at the desired

frequency. Since the system in this thesis has to meet the FCC 15 B standard, which regulates the signal starting from 0.15 MHz. While the system switching frequency is 40 kHz, so the first highest harmonic occurs at 0.16 MHz. Therefore, the desired frequency is selected as 0.16 MHz.

The transfer function is the LISN current over equivalent voltage, and the equivalent voltage does not change in the original circuit and the circuit with DM filter. Hence, the relation between the transfer functions and the FFT value can be expressed in following equation:

$$\left|\frac{\mathrm{TF}_o}{\mathrm{TF}_{DM}}\right| = \frac{\mathrm{FFT}_{f\_h\_o}}{\mathrm{FFT}_{f\_h\_DM}} \tag{3-20}$$

Here the $\mathrm{FFT}_{f\_h\_o}$ is the FFT value of the LISN current at 0.16 MHz in the original circuit, $\mathrm{FFT}_{f\_h\_DM}$ is the FFT value of the LISN current at 0.16 MHz in the circuit with DM filter, which is calculated from the FCC 15 B standard. Now the value of all the other three terms in the above equation are all known, so the first function of L and C, TF_{DM} , can be obtained.

There are lots of pairs of L and C which meet this function, so the next goal is to find that which filter also has the minimized volume.

Step 4: Capacitors are not customized, they only have certain values, and corresponds to certain volumes. According to the operating scenario of the rectifiers in this thesis, only nine capacitors are selected for comparison, which is shown in Table 8.

Table 8 Selected Capacitors for filter design

Part Number	C (μF)	VAC (V)	Volume (m3)
B25834F4225K1-ND	2.2	640	0.00003393
B25832F4475K1-ND	4.7	640	0.00005655
B25834L4106K9	10	600	0.00010807
B25834L4156K9	15	600	0.00016886
B25834D4226K4	22	600	0.00033666
B25834D4336K4	33	600	0.00051236
B25834D4476K9	47	600	0.00065137
B25834D4686K4	68	600	0.00080281
B25834D4107K4	100	600	0.00122178

For the inductor, the relation of volume and inductance has been given in the first section. Then the total volume of the DM filter can be obtained, which is a function of L and C. If the L and C are given, then the minimized volume of the DM filter can be calculated by comparing all the cases. Therefore, the second function of L and C is found.

Step 5: By solving the two functions of L and C given in step 3 and step 4, the L and C can be easily calculated, also the minimized volume is obtained at the same time.

3.2.2 CM EMI Filter Design

To design the CM filters for the three phase rectifiers, there are four steps.

1. Create equivalent CM circuit for the rectifiers with DM filter. Derive its transfer function.
2. Add CM filter to the circuit, and assume the relationships among the components. Create its equivalent CM circuit and derive the transfer function.
3. Measure the FFT at specific frequency, calculate the required maximum FFT value from the standards limitation, and use the transfer function from step 1 and step 2 to get a function of L and C.

4. Solve the function from step 3 to get the value of L for the filter.

The following part gives the detailed design process step by step.

Step 1: Given the original three-phase VSR and CSR as shown in Figure 3-7 and Figure 3-9, then the CM equivalent circuit can be obtained as shown in following figures [12] [13]:

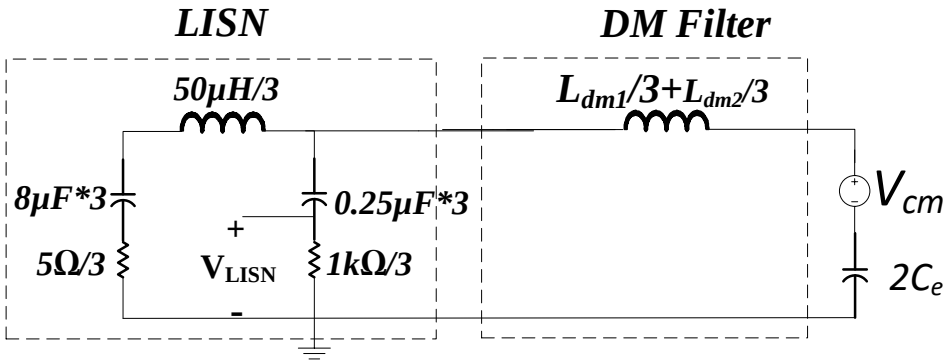

Figure 3-11 CM equivalent circuit for VSR without CM filter

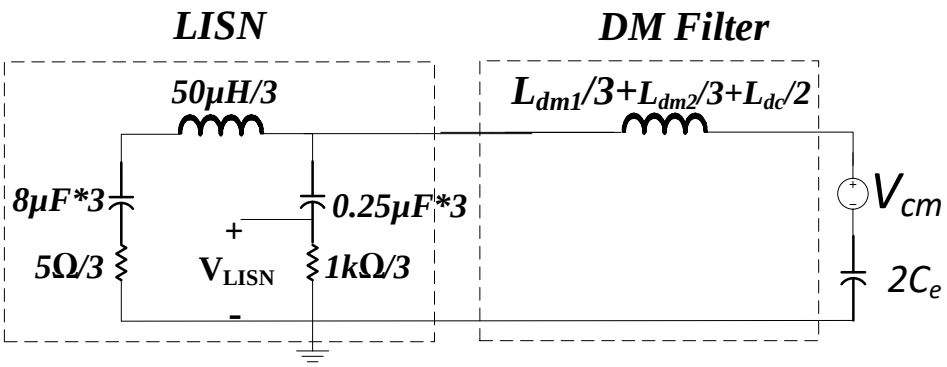

Figure 3-12 CM equivalent circuit for CSR without CM filter

With the equivalent circuit, the transfer function for VSR and CSR without CM filter are obtained in following equations:

$$\left|\mathrm{TF}_{VSRo\_CM\_}\right| = \left|\frac{I_{LISN}}{V_{o\_cm}}\right| = \left|\frac{s6C_e}{s^2 2(L_{dm1}+L_{dm2})C_e + 3}\right| \tag{3-21}$$

$$\left|\mathrm{TF}_{CSRo\_CM}\right| = \left|\frac{I_{LISN}}{V_{o\_cm}}\right| = \left|\frac{s6C_e}{s^2(2L_{dm1}C_e + 2L_{dm2}C_e + 3L_{dc}C_e) + 3}\right| \tag{3-22}$$

Based on the properties of the circuits, the LCL filter is selected as the CM filter For VSR, and CSR. The most inboard CM inductors are the largest in order to filter the EMI noise. The inductors are selected as $L_{cm2} = 3\ L_{cm1}$ for VSR, $L_{cm2} = 3\ L_{cm1}$ and $L_{cm2} = 4\ L_{cm1}$ for CSR. Then the new circuit and its CM equivalent circuit are given in following figures:

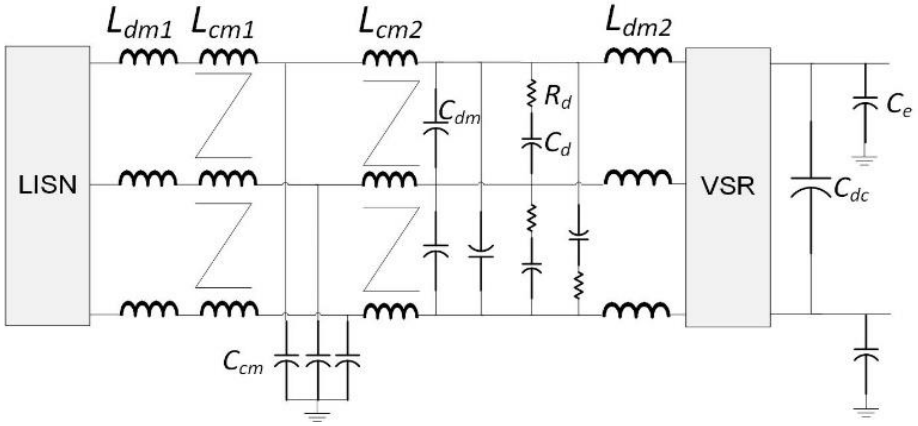

Figure 3-13 VSR with DM and CM filters

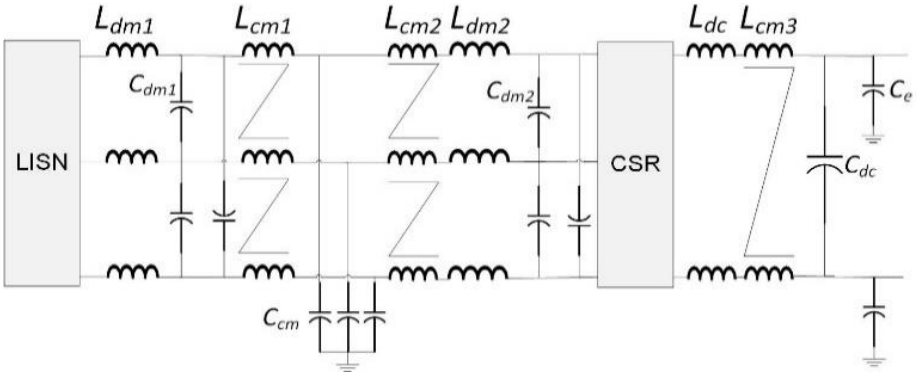

Figure 3-14 CSR with DM and CM filters

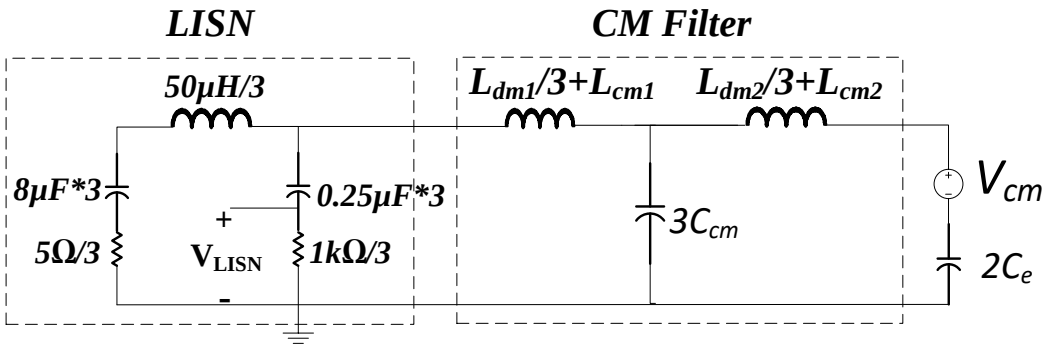

Figure 3-15 CM equivalent circuit of VSR with DM and CM filterS

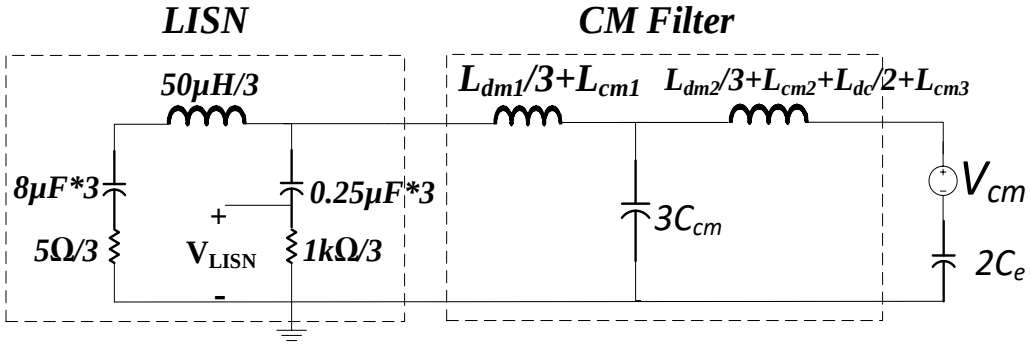

Figure 3-16 CM equivalent circuit of CSR with DM and CM filter

The transfer functions of the CM filters are expressed in following equations:

$$\left|\mathrm{TF}_{VSR_{CM}}\right| = \left|\frac{I_{LISN}}{V_{cm}}\right| = \left|s2C_e/(s^4 6C_{cm}C_e(\frac{L_{dm1}}{3} + L_{cm1})(L_{cm2} + L_{cm3}) + s^2(3C_{cm}\left(\frac{L_{dm1}}{3} + L_{cm1}\right) + 2C_e(L_{cm2} + L_{cm3})) + 1)\right| \quad (3\text{-}23)$$

$$\left|\mathrm{TF}_{CSR\_CM}\right| = \left|\frac{I_{LISN}}{V_{cm}}\right| = \left|s2C_e/(s^4 6C_{cm}C_e(\frac{L_{dm1}}{3} + L_{cm1})(L_{cm2} + L_{cm3} + L_{dc}/2 + L_{dm2}/3) + s^2(3C_{cm}\left(\frac{L_{dm1}}{3} + L_{cm1}\right) + 2C_e(L_{cm2} + L_{cm3} + L_{dc}/2 + L_{dm2}/3)) + 1)\right| \quad (3\text{-}24)$$

Step 3: Run the simulation model of VSR and CSR without CM filter, measure the CM current through LISN, calculate the FFT of the current. Find the absolute FFT value of the current at 0.16 MHz. Then calculate the FFT value at the same frequency from the FCC 15 B standard. The relation between the transfer functions and the FFT values can be expressed in Equation 3-9.

$$\left|\frac{\mathrm{TF}_o}{\mathrm{TF}_{CM}}\right| = \frac{\mathrm{FFT}_{f\_h\_o}}{\mathrm{FFT}_{f\_h\_CM}} \tag{3-25}$$

Here the $\mathrm{FFT}_{f\_h\_o}$ is the FFT value of the LISN CM current at 0.16 MHz in the original circuit, $\mathrm{FFT}_{f\_h\_CM}$ is the FFT value of the LISN CM current at 0.16 MHz in the circuit with CM filter, which is calculated from the FCC 15 B standard.

Step 4: Solve the function to get the value of L for the filter. Now the value of all the other three terms in the above equation are all known, so the L can be obtained. Therefore, the CM filter is designed.

4 Comparison of the VSR and CSR

With the details of filter design provided by the previous chapter, this chapter gives the volume, loss calculation, and the comparison of the VSR and CSR.

4.1 Volume calculation

In order to quantify the impacts that SiC devices have on power density, it is necessary to calculate the total volume of the system. First, from Section 3.2, the minimized inductor volume can be calculated by giving the inductance. Second, the capacitor volume can be found in Table 8. Third, by solving the DM transfer functions, different pairs of L and C can be obtained. Then the volume of those DM filters can be calculated. Also, the volume of CM filter can be calculated by solving the CM transfer function. Last, the heat sink size can be calculated by giving the total loss of the filter. The heatsink size depends on the loss of inverters, the larger the loss, the bigger the heatsink size. According to the loss calculated from the next section, the size of the heatsink can be approximately calculated. Therefore, the optimized filter design can be obtained, which are shown in following figures.

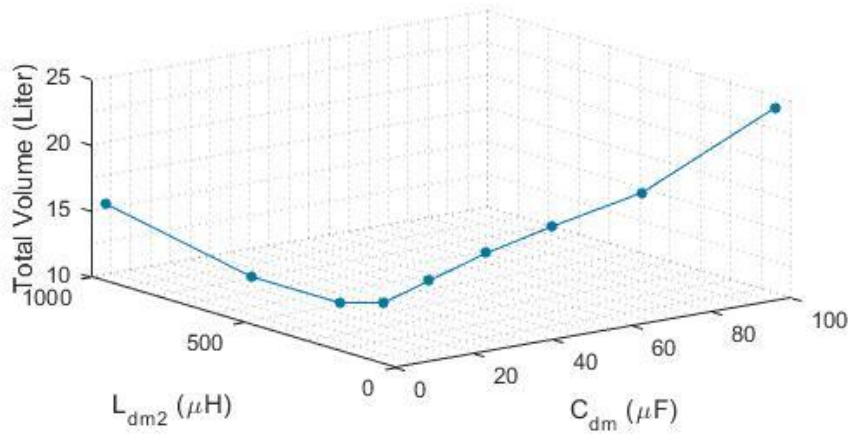

Figure 4-1 L_{dm2} and C_{dm} values for designing filters for VSR

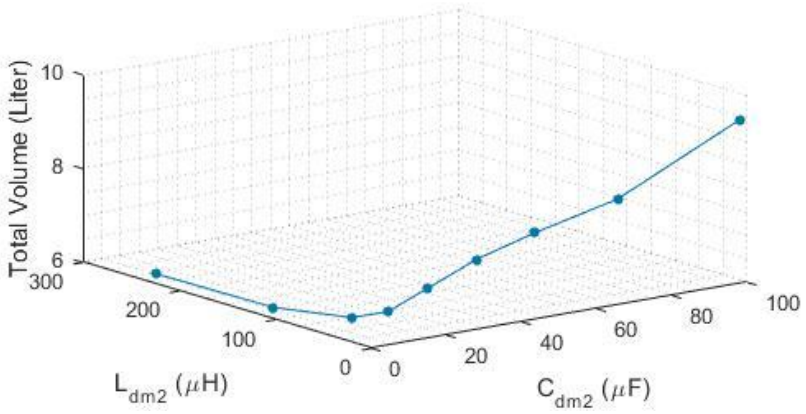

Figure 4-2 L_{dm2} and C_{dm2} values for designing filters for CSR

In Figure 4-1, the third point corresponds to the minimum volume. Therefore, the third case is selected as the final design, which corresponds to V_{DM}=7.5 L, V_{CM}=1.8 L, $V_{heatsink}$ =3.0 L.

From Figure 4-2, the second point corresponds to the minimum volume. Therefore, the second case is selected as the final design, which corresponds to V_{DM}=2.0 L, V_{CM}=0.8 L, $V_{heatsink}$ =3.3 L.

With the given volume for DM filter, CM filter and heatsink, the total volume of the rectifiers can be obtained as:

$$V_{VSR} = V_{DM,VSR} + V_{CM,VSR} + V_{heatsink,VSR} = 14.3\ L \tag{4-1}$$

$$V_{CSR} = V_{DM,VSR} + V_{CM,VSR} + V_{heatsink,VSR} = 6.1\ L \tag{4-2}$$

4.2 Loss Calculation

The previous section has given the procedure for volume calculation. Therefore, with the obtained size of inductor, the weight can be calculated, and also the size of the copper wire can be calculated. The loss of all the capacitors is so small that it is neglected. Only the inductor and copper loss will be calculated in the following.

For the calculation of core loss density, the power law equation [14] is applied as shown in following equations:

$$P_{vo} = k{f_o}^{\alpha}{B_o}^{\beta} \tag{4-3}$$

$$P_{vh} = 4k{f_{sw}}^{\alpha}{B_h}^{\beta} \tag{4-4}$$

For the inductors designed in this thesis, metglas is selected as the core material. According the data provided by the manufacturer, k= 6.5, α = 1.51 and β=1.74. P_o is the core loss density at the fundamental frequency. P_h is the core loss density at harmonic frequencies. B_o is the magnetic flux density at the fundamental frequency. B_h is the magnetic flux at the harmonic frequency, which is estimated to be 3% of B_o. The magnetic flux density is different between DM filter loss calculation and CM filter loss calculation. The magnetic flux results from the DM current and CM current correspondingly. After the core loss densities are obtained, with the volume of the core, then the filter core loss can be calculated by multiplying the density with volume as shown blow:

$$P_{core} = (P_{vo} + P_{vh})V_{core} \tag{4-5}$$

The given resistance of copper is specified at a temperature of 20 ^oC, the resistance values for other temperature other than the standard one can be determined by the following formula:

$$R = R_{ref}[1 + \alpha(T - T_{ref}) \tag{4-6}$$

The inductor working temperature in the thesis is assumed to be around 180 ^oC, so T=180. α is the temperature coefficient of resistance for the conductor material, here copper is selected as the conductor, so α= 0.00386. Since the copper length and size have been calculated in the last section, then the copper loss can be determined by the following equation:

$$P_{copper} = {I_{rms}}^2 R \tag{4-7}$$

Then the filter loss is determined by the following equation:

$$P_{filter} = P_{core} + P_{copper} \quad (4\text{-}8)$$

With the above equations, it is obtained that the DM filter loss of VSR and CSR are 438.2 W and 300.4 W, their CM filter loss is 179.8 W and 95.0 W. Therefore, the total filter loss of VSR and CSR are 618.0 W and 395.4 W.

4.2.1 Calculation for SiC MOSFET device Losses

Based on the system rating, CREE CAS120M12BM2 [4] is selected as the switching device due to the following advantages:

- Ultra low loss
- High-Frequency Operation
- Zero Reverse Recovery Current from Diode
- Zero Turn-off Tail Current from MOSFET

In order to quantify the impacts that SiC MOSFET devices have on the power density and efficiency on the whole system, this section describes the process for calculating the losses in the SiC MOSFET devices.

MOSFET Loss

In the PLECS block of circuits, a thermal description was created for each device according to the data sheet of CREE CAS120M12BM2. Figure 4-3 through Figure 4-5 show the curves of different loss of MOSFET.

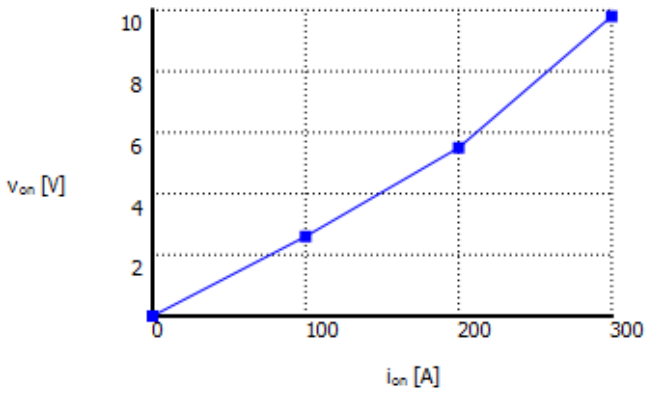

Figure 4-3 Thermal description of MOSFET (conduction loss)

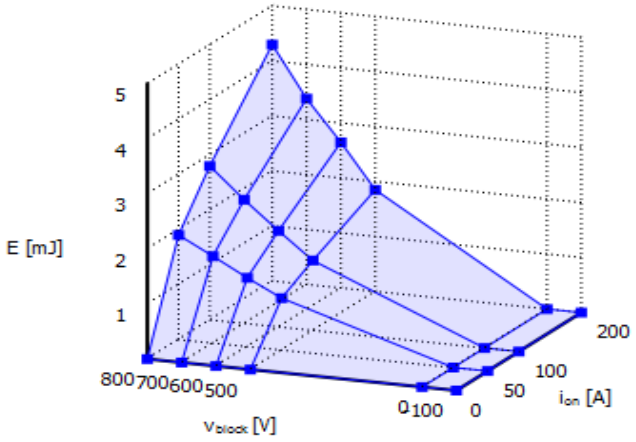

Figure 4-4 Thermal description of MOSFET (turn-on loss)

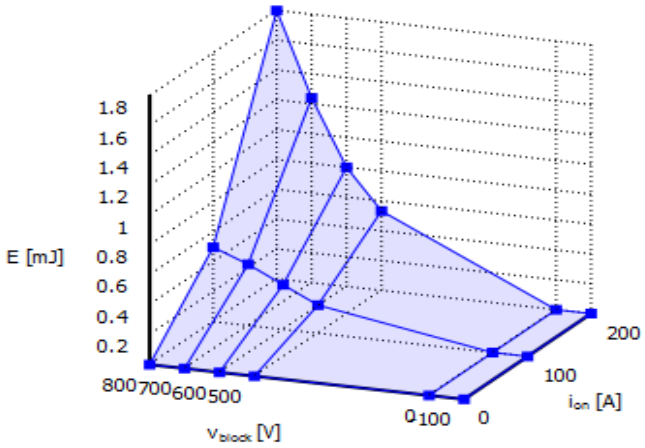

Figure 4-5 Thermal description of MOSFET (turn-off loss)

From datasheet of CREE CAS120M12BM2, the curves at 25℃ and 150℃ can be obtained, while the converters work at 125℃, the data at this temperature can be calculated using linear interpolation from the curves in the thermal description. A probe was added to measure the instantaneous loss, and an average semiconductor loss calculation block was used to calculate the losses.

By running the Simulation model of VSR, the instantaneous conduction loss and switching loss of MOSFET are given in Figure 4-6.

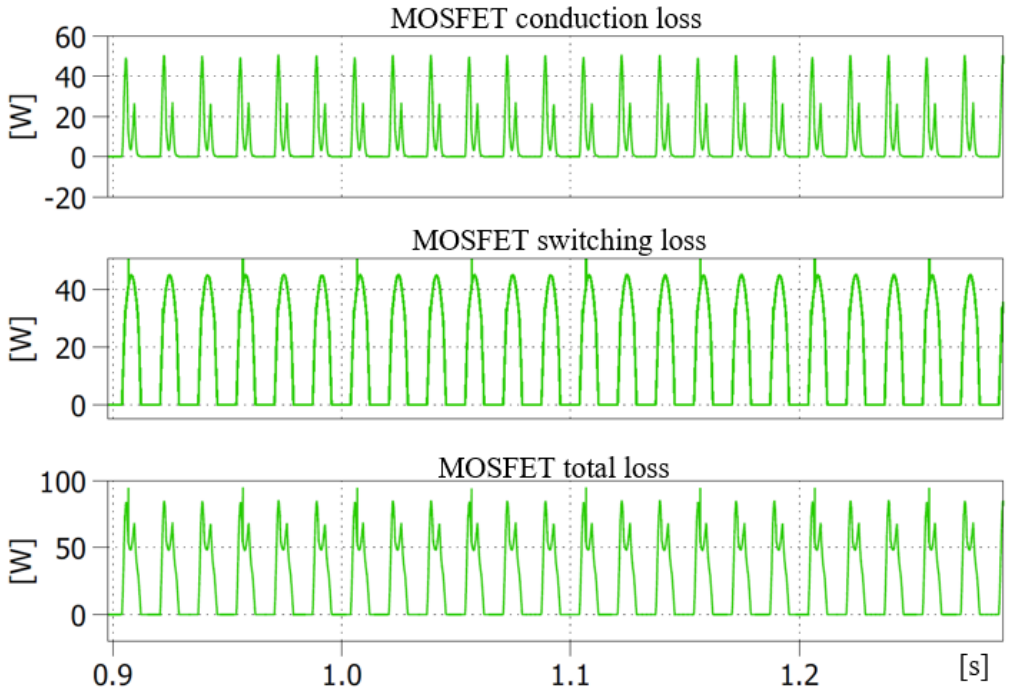

Figure 4-6 Instantaneous conduction and switching loss of MOSFET in VSR

In the above figure, the first curve in this figure is the conduction loss, the second is the switching loss, and the last is the addition of the first one and second one, which is the total loss of MOSFET.

Hence, by calculating the average value of the first and second curves, the average value of the total loss can be obtained. The average value is defined in following:

$$f_{avg}(t, t+T) = \frac{\int_t^{t+T} f(x)dx}{T} \tag{4-9}$$

In the simulation of VSR, the fundamental frequency is 60 Hz, so the period is $\frac{1}{60}\ s$. Since the signal is the same in every period at stable state, the average value can be obtained in one period. Solving the equation with value given by above figure yields the results that the average conduction loss is 7.24 W, average switching loss is 16.12 W, the average loss of MOSFET is:

$$P_{MOSFET,VSR} = P_{conduction,M,VSR} + P_{switching,M,VSR} = 23.34\ W \tag{4-10}$$

By running the Simulation model of CSR, the instantaneous conduction loss and switching loss of MOSFET are given in Figure 4-7.

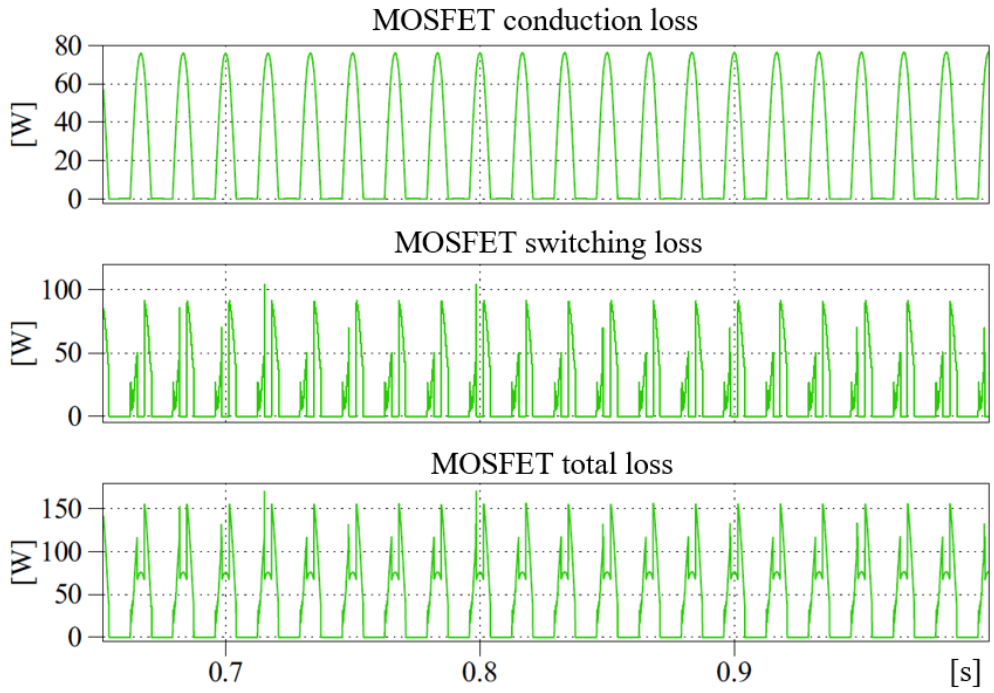

Figure 4-7 Instantaneous conduction and switching loss of MOSFET in CSR

Solving the average equation with value given by above figure yields the results that the average conduction loss is 24.52 W, average switching loss is 14.59 W. Hence the average loss of MOSFET is:

$$P_{MOSFET,VSR} = P_{conduction,M,V} + P_{switching,M,V} = 39.11\,W \quad (4\text{-}11)$$

Diode Loss

In the PLECS block of circuits, a thermal description of the diodes was also created according to the data sheet of CREE CAS120M12BM2. The turn-on loss of diode is very small, so it is ignored. Also, due to the zero reverse recovery current from the diode, the turn-off loss of diode is zero. Thus, only the curve of conduction loss is given, and it is shown in the figure below.

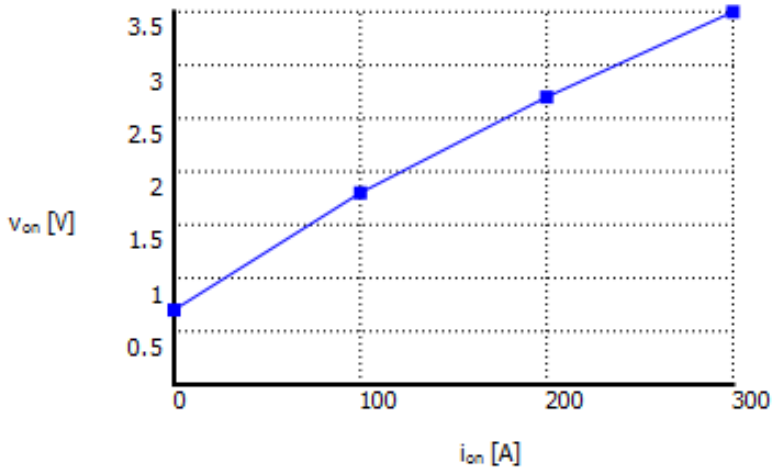

Figure 4-8 Thermal description of Diode (conduction loss)

By running the Simulation model of VSR, the instantaneous conduction loss and switching loss of diode is given in Figure 4-9.

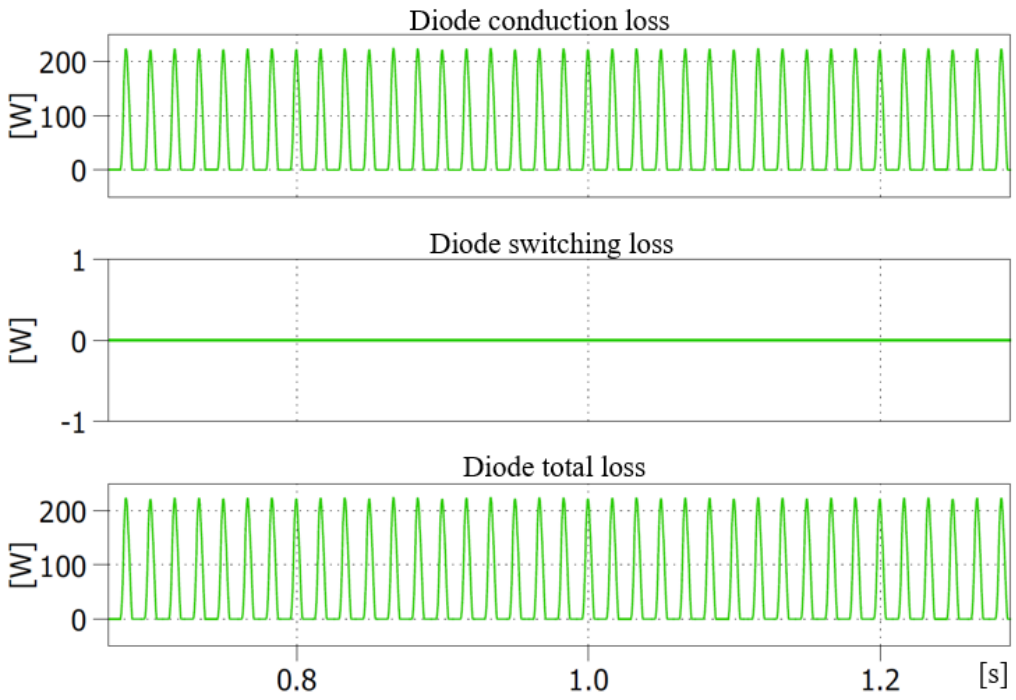

Figure 4-9 Instantaneous conduction and switching loss of Diode in VSR

Solving the average equation with the value given by above figure yields the results that the average conduction loss is 56.21 W, average switching loss is 0 W. Hence the average loss of MOSFET is:

$$P_{Diode,VSR} = P_{conduction,D,VSR} + P_{switching,D,VSR} = 56.64\,W \qquad (4\text{-}12)$$

While for CSR, there are two different kinds of diodes. One is in series with the SiC devices, and the other is the freewheeling diode. By running the Simulation model of CSR, the instantaneous conduction loss and switching loss of series and freewheeling diodes are given in Figure 4-10 and Figure 4-11 correspondingly.

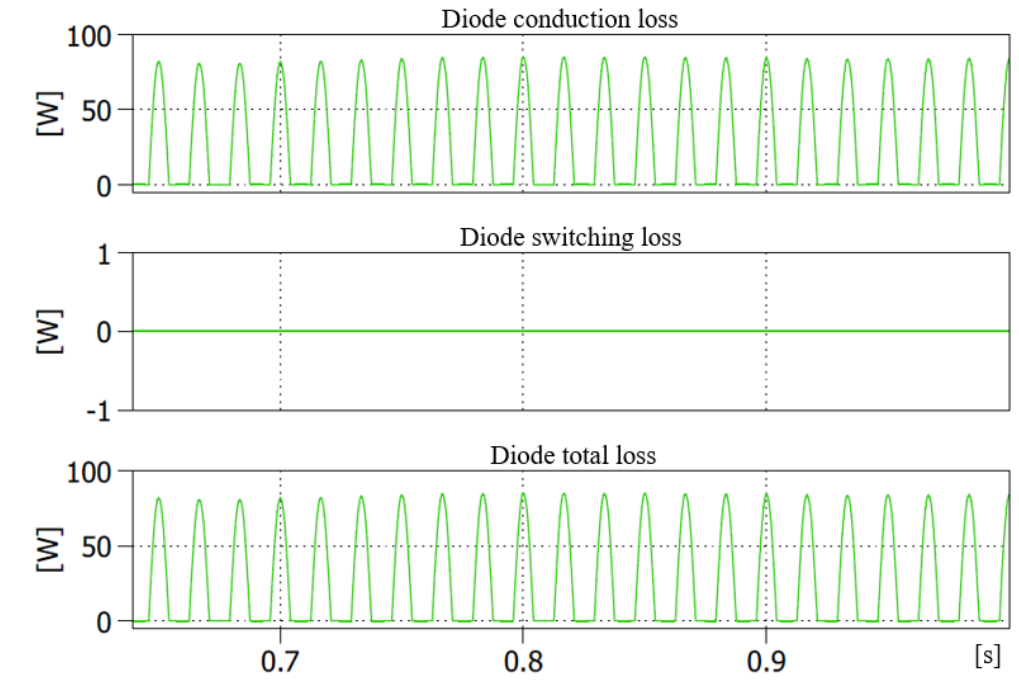

Figure 4-10 Instantaneous conduction and switching loss of series diode in CSR

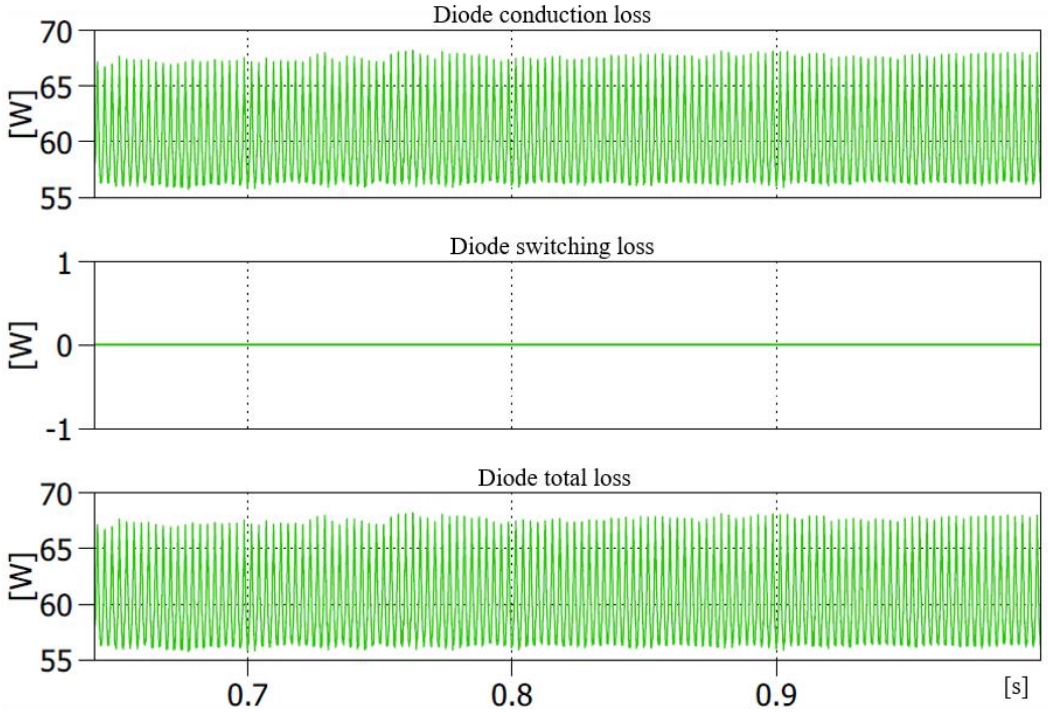

Figure 4-11 Instantaneous conduction and switching loss of freewheeling diode in CSR

Solving the average equation yields the results that the average conduction loss for the series diode is 26.81 W, average switching loss is 0 W. Hence the average loss of series diode is:

$$P_{sDiode,CSR} = P_{conduction,sD,CSR} + P_{switching,sD,CSR} = 26.81\ W \quad (4\text{-}13)$$

Solving the average equation yields the results that the average conduction loss for the freewheeling diode is 60.30 W, average switching loss is 0 W. Hence the average loss of freewheeling diode is:

$$P_{fDiode,CSR} = P_{conduction,fD,CSR} + P_{switching,fD,CSR} = 60.30\ W \quad (4\text{-}14)$$

After getting the loss of each MOSFET and diode, the total switching device loss can be obtained in Equation 4-9 and Equation 4-10.

Therefore, the total switching device loss for VSR is:

$$P_{SD,VSR} = \left(P_{MOSFET,VSR} + P_{Diode,VSR}\right) * 6 = 479.88\ W \quad (4\text{-}15)$$

The total switching device loss for CSR is:

$$P_{SD,CSR} = \left(P_{MOSFET,CSR} + P_{sDiode,CSR}\right) * 6 + P_{fDiode,CSR} = 455.82\ W \quad (4\text{-}16)$$

4.2.2 Total Loss

For the VSR and CSR system, only the loss of switching device and filter is calculated, the loss of wire besides that in the filter is neglected, and loss of other components are also ignored, since they are very low compared with the switching device loss and filter loss. Since each loss has been obtained in the previous section, the total loss can be calculated in following equation.

For the VSR, the total loss is:

$$P_{VSR} = P_{SD,VSR} + P_{filter,VSR} = 1098.0\ W \tag{4-17}$$

For the CSR, the total loss is:

$$P_{CSR} = P_{SD,CSR} + P_{filter,CSR} = 851.2\ W \tag{4-18}$$

The loss of VSR and CSR is then summarized in Table 5-9.

Table 9 The loss Summary of VSR and CSR

	VSR	CSR	Units
Filter loss	618.0	395.4	W
Switching Device loss	480.0	455.8	W
Total loss	1098.0	851.2	W

Form the Table 9, the filter loss of VSR is much higher than CSR, this is mainly because of that ac input side voltage of VSR is much lower than that of CSR, then the input side ac current is higher than that of CSR. The higher current leads to higher filter loss for VSR. While the switching device loss of VSR is a little higher than that CSR. This is because of the topology of CSR. Compared with the switching devices of VSR, CSR has seven more diodes, in which six diodes are in series with each MOSFET, and the 1 is the freewheeling diode. The six series diodes are used to prevent current flow back to the current source, and the freewheeling diode is applied for allowing the DC link inductor current to freewheel through it. Since the diodes have a lot of conduction loss, which results in the high switching device loss for CSR. The CSR has lower loss both in switching device and filter. Thus the total loss of CSR is lower than VSR.

4.3 Power Density

In this thesis, the power converters are designed with the same output power, which is the rated power. Therefore, the input power is the addition of the rated power and the loss in the converter. The power density of the rectifiers can be calculated as:

$$PowerDensity_{VSR} = \frac{P_{in,VSR}}{V_{VSR}} = \frac{P_{rated,VSR} + P_{loss,VSR}}{V_{VSR}} = 2.2\ L \tag{4-19}$$

$$PowerDensity_{CSR} = \frac{P_{in,CSR}}{V_{CSR}} = \frac{P_{rated,CSR} + P_{loss,CSR}}{V_{CSR}} = 5.1\ L \tag{4-20}$$

4.4 Energy Efficiency

The efficiency of the rectifiers can be calculated by the following equation:

$$\eta = \frac{P_{rated}}{P_{in}} = \frac{P_{rated}}{P_{rated} + P_{loss}} \tag{4-21}$$

The rated power for VSR and CSR are the same, which is 30 kW. The total power loss of VSR and CSR are 1098.0 W and 851.2 W. Thus the efficiency of VSR and CSR are 96.5% and 97.2%. This shows that CSR has a slightly higher efficiency than VSR.

4.5 Summary

Table 10 provides the information about the values of the components used in designing the filters and also the calculated parameters of the rectifiers. Comparison of the calculated efficiency and power density of the two rectifiers shows the superiority of the CSR compared to the VSR [15].

Table 10 Operating scenario and calculated parameters of the rectifiers

	VSR	**CSR**	**Units**
$\mathbf{P_{rated}}$	30	30	kVA
$\mathbf{V_{llrms}}$	208	480	V
$\mathbf{I_{rms}}$	83.3	36.1	A
$\mathbf{I_{peak}}$	117.8	51.0	A
$\mathbf{V_{dc}}$	350	350	V
$\mathbf{I_{dc}}$	85.7	85.7	A
$\mathbf{R_{load}}$	4.1	4.1	Ω
$\mathbf{L_{dm1}}$	62.4	6	µH
$\mathbf{L_{dm2}}$	312	120	µH
$\mathbf{C_{dm1}}$	10	0.5	µF
$\mathbf{C_{dm2}}$	NA	4.7	µF
$\mathbf{C_{d}}$	30	NA	µF
$\mathbf{R_{d}}$	2.5	NA	Ω
$\mathbf{L_{cm1}}$	6.3	1.4	mH
$\mathbf{L_{cm2}}$	18.9	4.2	mH
$\mathbf{L_{cm3}}$	NA	5.6	mH
$\mathbf{C_{cm}}$	0.5	0.5	µF
$\mathbf{L_{dc}}$	NA	0.25	mH
$\mathbf{C_{dc}}$	3000	150	µF
Total Volume	14.3	6.1	Liter
Filter Loss	618	395.4	W
Switching Device Loss	480	455.8	W
Total Loss	1098	851.2	W
Power Density	2.2	5.1	kW/L
Efficiency	96.5%	97.2%	1

From the table above, it can be obtained that operating at 40kHz, the loss of the SiC device of CSR is a little lower than that of VSR, the filter loss of CSR is much lower than that of VSR, and the volume of CSR is much smaller than that of VSR. The CSR has slightly higher efficiency, but much higher power density than VSR.

5 PWM Methods

For the VSR, the Third Harmonic Injection PWM control is applied. This modulation method has the minimum number of switch commutations, and thus ensuring the minimum filter size for a given switching frequency.

For the CSR, there are two cases of operation modes which are addressed in following sections. One is the continuous operation mode, and the other is the discontinuous operation mode. Even though the CSR in this thesis is working at continuous mode, the discontinuous case is still worthy mentioned of future work. When the load is light, dc-link current can be very high. Even though there is some current ripple, the output current is still continuous since the ripple is still small compared with the average value. While the system goes into discontinuous operation mode when the load is heavy. This is because of that the current ripple is relatively quite large with respect to the average dc-link current. Therefore, this chapter presents the modulation methods for the CSR operating in continuous mode, also addresses a new modulation strategy to deal with the discontinuity operation mode to ensure nearly sinusoidal current. And the modulation methods for CSR addressed in this chapter are all in SVPWM point of view. Even though the discontinuous conduction mode is not considered in the comparison of VSR and CSR, it is a valuable work, which can be used in more complex conditions, such as the system requiring power ramp rate control.

5.1 Third harmonic injection methodology of VSR

The Third Harmonic Injection PWM control is employed in the VSR because of the minimum number of switch commutations. In the simulation model of VSR, the third harmonic value is:

$$v_{ref} = \frac{\min(V_a, V_b, V_c) + \max(V_a, V_b, V_c)}{\sqrt{3}} \tag{5-1}$$

With the above instantaneous third harmonic value, the phase voltages are given in the following:

$$v_{a,new} = v_a - v_{ref} \tag{5-2}$$

$$v_{b,new} = v_b - v_{ref} \tag{5-3}$$

$$v_{c,new} = v_c - v_{ref} \tag{5-4}$$

A snapshot of the third harmonic injection model is shown in Figure 5-1, and the simulated result is shown in Figure 5-2.

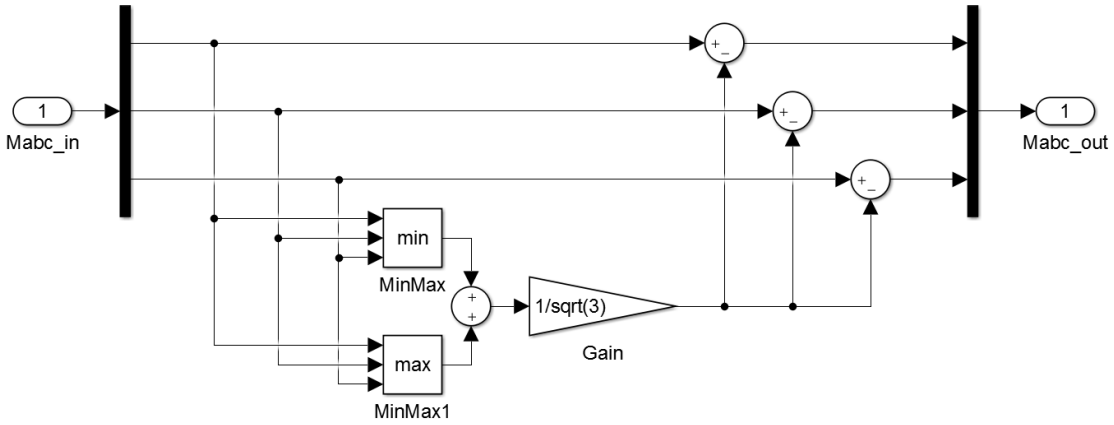

Figure 5-1 Simulation model of third harmonic injection

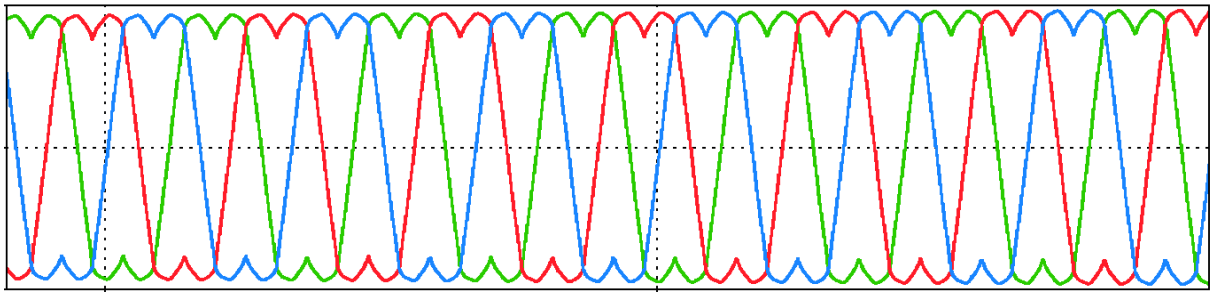

Figure 5-2 Simulated third harmonic voltage

The initial sinusoidal voltage waveform is modified by the third harmonic injection. The third harmonic gives more dynamic range to drive out harmonics. This control strategy provides the

modulation index up to 1.15, thus increasing the output dc voltage. There is some downside of this strategy due to the injection of third harmonic common mode current into the circuit. But the impedance at third harmonic is very large, so the common mode current at this frequency is very low, which does not impact the core size of common mode inductor.

5.2 Continuous Operation Mode of CSR

The CSR modulation strategy utilizes the six-pulse symmetry of the circuit. Since each cycle corresponds to 360^{o}, each sector is a 60^{o} interval as in Figure 5-3, which describes the sector 2, and it means that switch S2 is always on, S1 S3 and S5 are on or off depending on the duty cycles.

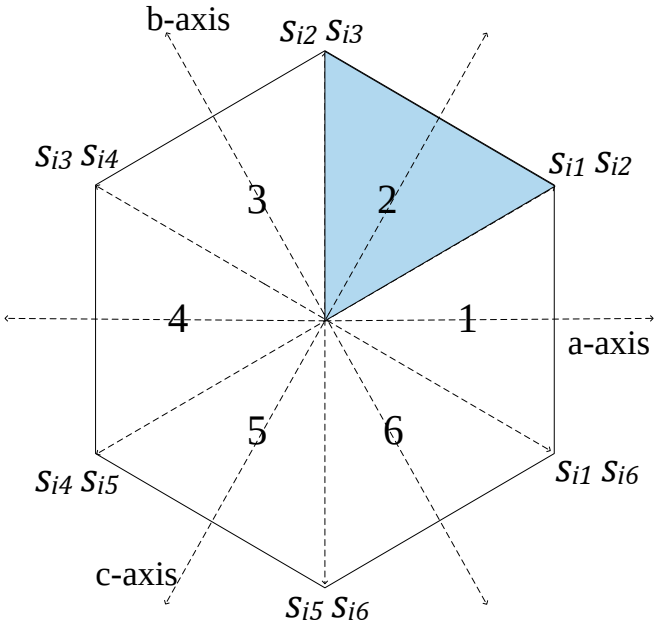

Figure 5-3 CSR switch states

In Figure 5-4, the path of the dc-link inductor current from source to load during a switching period is expressed in three states, and the active power semiconductors of the converter are also included in the path. In this presentation, k n and z switch states correspond to the power transfer state from a line to line voltage to another.

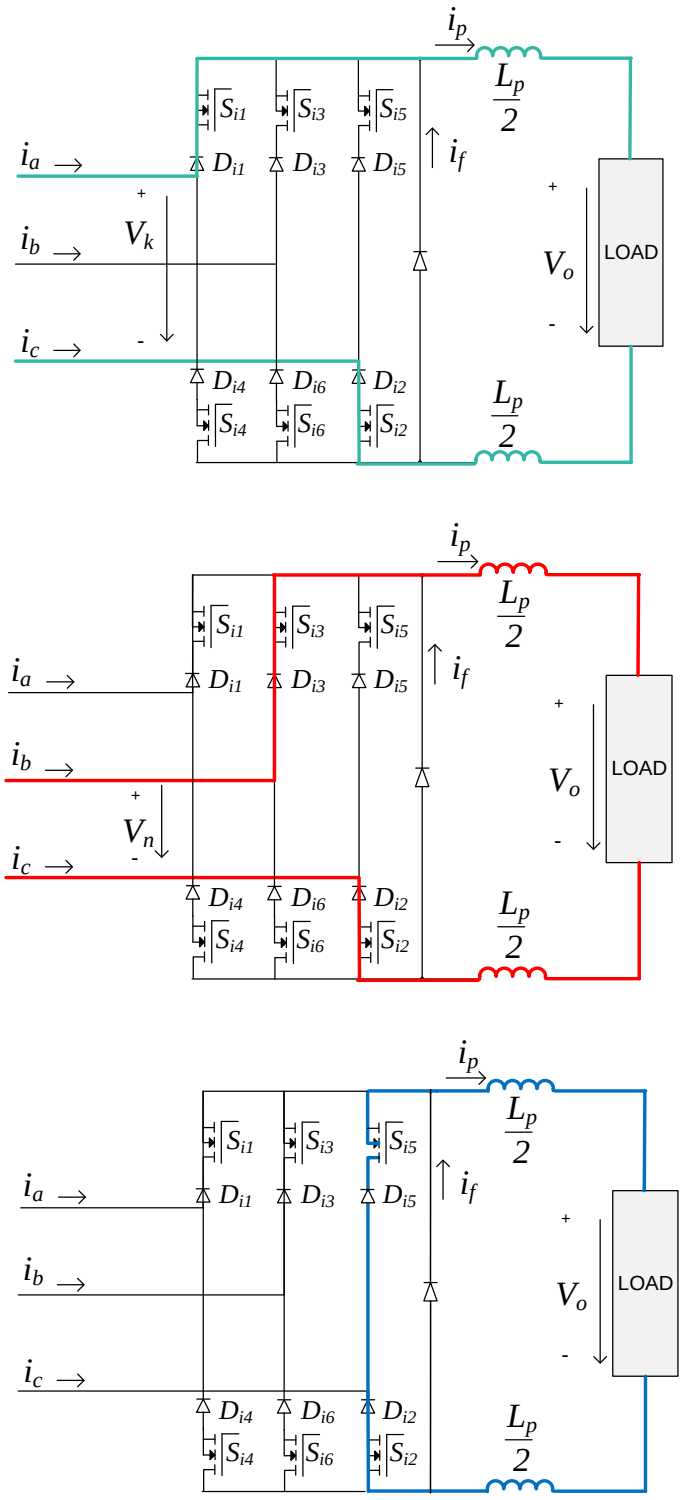

Figure 5-4 CSR switch states in sector 2: (a) k state, (b) n state, (c) z state

In each sector, the line to neutral voltages are:

$$v_{k0} = \frac{V_i}{\sqrt{3}} \sin(\frac{\pi}{3} - \varphi_i) \tag{5-5}$$

$$v_{n0} = \frac{V_i}{\sqrt{3}} \sin(\varphi_i) \tag{5-6}$$

The modulation index m_i is:

$$m_i = \frac{2}{\sqrt{3}} \frac{v_0}{v_i} \tag{5-7}$$

Thus, the duty ratios of k n and z state are:

$$d_k = m_i \sin(\frac{\pi}{3} - \varphi_i) \tag{5-8}$$

$$d_n = m_i \sin(\varphi_i) \tag{5-9}$$

$$d_z = m_i \left(1 - \sin\left(\frac{\pi}{3} - \varphi_i\right) - \sin(\varphi_i)\right) \tag{5-10}$$

The above equations of duty ratio calculation only apply to the continuous operation mode. For the case of discontinuous operation study, the following section addresses the new modulation strategies to deal with it and ensures the nearly sinusoidal current for CSR.

5.3 Discontinuous Operation Mode of CSR

This section addresses two different modulation patterns. One is the Half-Symmetrical Modulation (HSM), and the other is the Full-Symmetrical Modulation (FSM). The difference between the two methods is the order of k n and zero states, and the placement of the freewheeling states within the switching period. The following derivation assumes the buck-buck voltage mode.

5.3.1 Half-Symmetrical Modulation (HSM)

As shown in Figure 5-5, the HSM divides the total switching period into equal parts. The k state turns on at first half part, and the n state turns on at the second half part. When the line-to-line voltage is higher than the output voltage, current increases. And when it is in the dwelling state, current decreases.

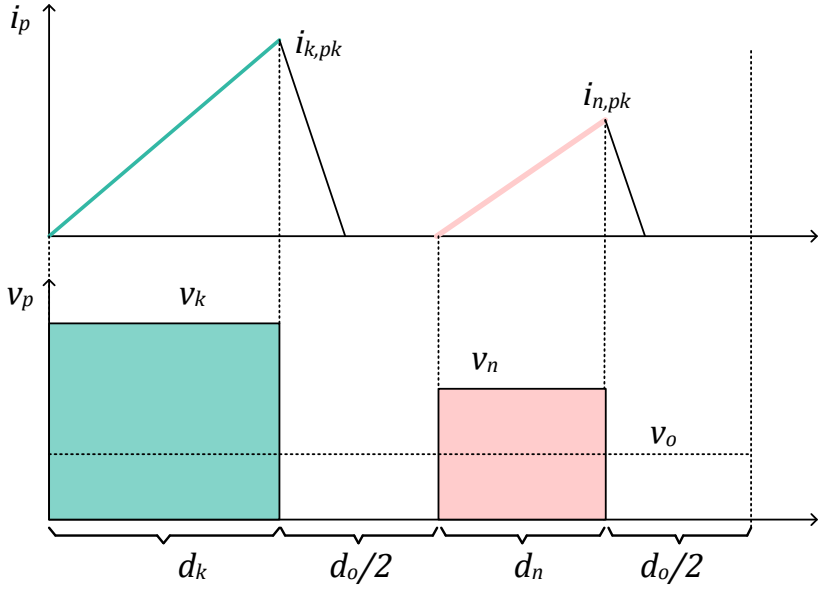

Figure 5-5 CSR HSM DCM

Given the estimate of dc-link inductance L_p and the switching frequency f_{si}, the following expressions can be found:

$$i_{k,pk} = \frac{(v_k - v_o)d_k}{L_p f_{si}} \tag{5-11}$$

$$i_{n,pk} = \frac{(v_n - v_o)d_n}{L_p f_{si}} \tag{5-12}$$

$$\langle i_k \rangle = \frac{i_{k,pk} d_k}{2} \tag{5-13}$$

$$\langle i_n \rangle = \frac{i_{n,pk} d_n}{2} \tag{5-14}$$

$$v_k d_k + v_n d_n = v_o(d_k + d_n + d_o) \tag{5-15}$$

Among the above equations, the first two derivate from the volt-second balance principle. By solving these equations, the duty ratios can be expressed as:

$$d_k = \sqrt{\frac{2L_p f_{si}\langle i_k \rangle}{v_k - v_o}} \tag{5-16}$$

$$d_n = \sqrt{\frac{2L_p f_{si}\langle i_n \rangle}{v_n - v_o}} \tag{5-17}$$

The switching waveform implantation is shown in the figure below:

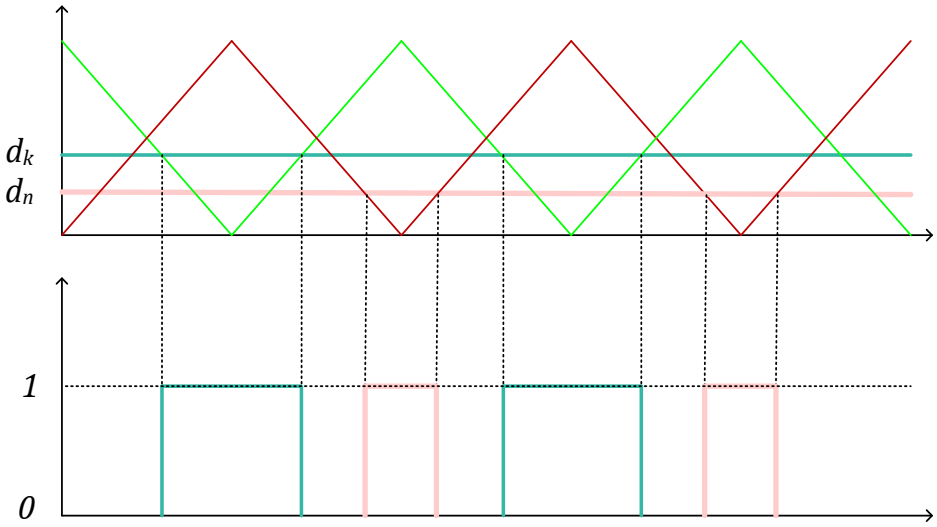

Figure 5-6 CSR HSM DCM switching waveform

The simulation result is shown in Figure 5-7. The first one is the ac side current, which is almost a sinusoidal wave, this testifies that the modulation method works well. The second one is the switching state. And the third one is the duty ratio of k and n states, which are calculated from Equation 5-16 and 5-17. Figure 5-8 shows the details of the circled part in the switching state.

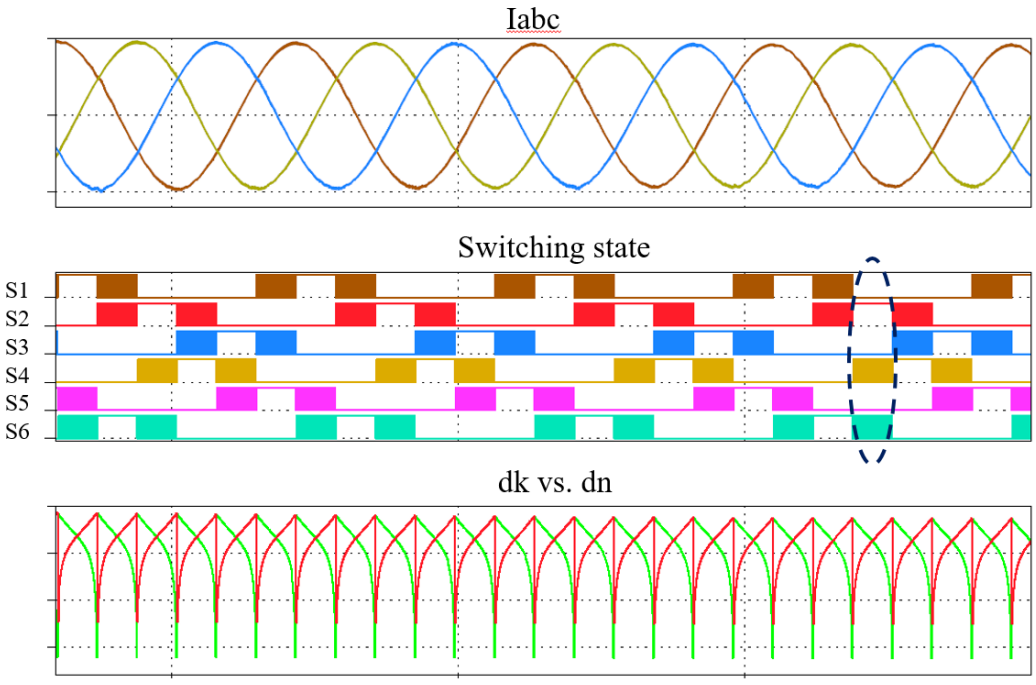

Figure 5-7 CSR HSM DCM

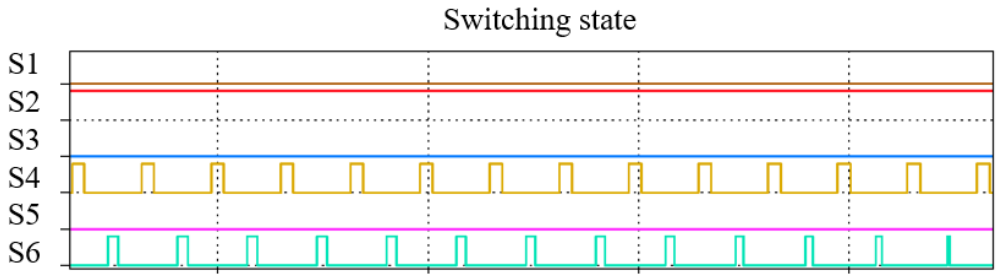

Figure 5-8 CSR HSM DCM detail

It is obvious that during a switching period, there is one switch which is on all the time, and there are two other switches, one is turned at the beginning of the switching period, and the other is turned on at half of the period.

5.3.2 Full-Symmetrical Modulation (FSM)

Compared with HSM, FSM keeps the active states adjacent. HSM has lower average dc-link current ripple. While FSM has the advantages of less switching loss because of the fewer device commutations [16]. Therefore, FSM tends to be the preferred approach for CSR. As shown in Figure 5-9, when k state turns off, n state turns on immediately. The dwelling state comes after the active states.

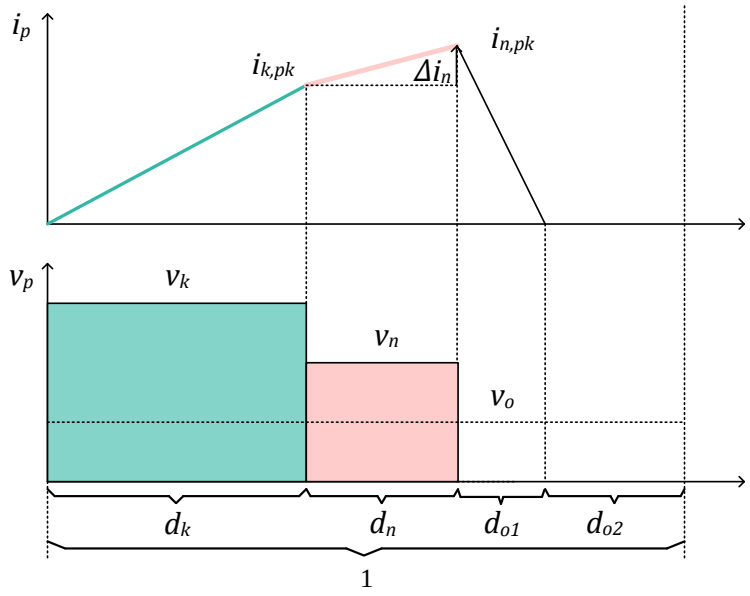

Figure 5-9 CSR HSM DCM

Given the estimate of dc-link inductance L_p and the switching frequency f_{si}, the following expressions can be found:

$$i_{k,pk} = \frac{(v_k - v_o)d_k}{L_p f_{si}} \tag{5-18}$$

$$i_{n,pk} = \frac{v_o d_{o1}}{L_p f_{si}} \tag{5-19}$$

$$\Delta i_n = \frac{(v_n - v_o)d_n}{L_p f_{si}} \tag{5-20}$$

$$\langle i_k \rangle = \frac{i_{k,pk} d_k}{2} \tag{5-21}$$

$$\langle i_n \rangle = (\frac{\Delta i_n}{2} + i_{k,pk}) d_n \tag{5-22}$$

$$v_k d_k + v_n d_n = v_o (d_k + d_n + d_{o1} + d_{o2}) \tag{5-23}$$

Among the above equations, the first three derivate from the volt-second balance principle. By solving these equations, the duty ratios can be expressed as:

$$d_k = \sqrt{\frac{2 L_p f_{si} \langle i_k \rangle}{v_k - v_o}} \tag{5-24}$$

$$d_n = \frac{\sqrt{2 \langle i_k \rangle (v_k - v_o) L_p f_{si}}}{v_n - v_o} \left(-1 + \sqrt{1 + \frac{(v_n - v_o) \langle i_n \rangle}{(v_k - v_o) \langle i_k \rangle}} \right) \tag{5-25}$$

The switching waveform implantation is shown in the figure below:

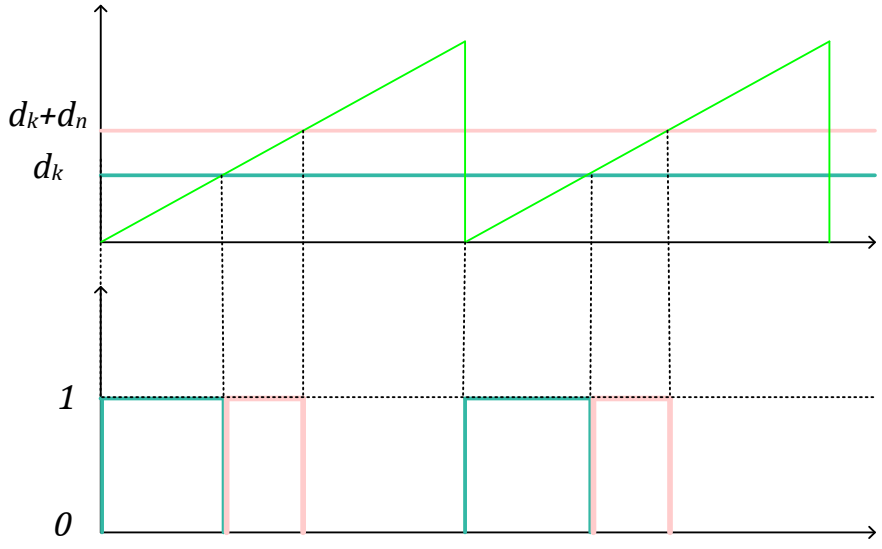

Figure 5-10 CSR FSM DCM switching waveform

The simulation result is shown in Figure 5-11. The first one is the ac side current, which is almost a sinusoidal wave, this testifies that the modulation method works well. The second one is the switching state. And the third one is the duty ratio of k and n states, which are calculated from Equation 5-24 and 5-25. Figure 5-12 shows the details of the circled part in the switching state.

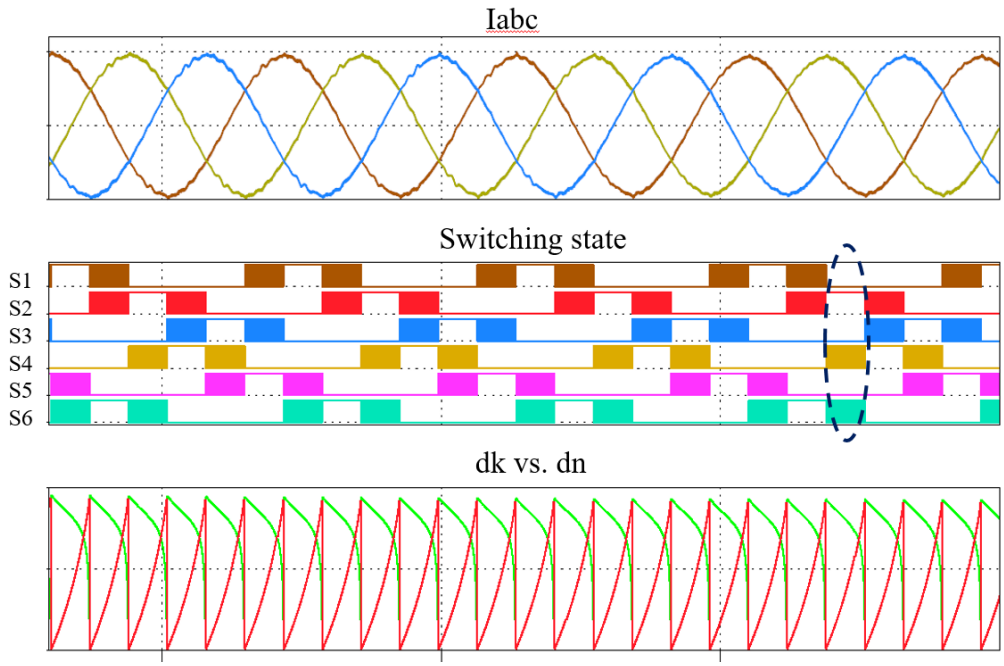

Figure 5-11 CSR FSM DCM

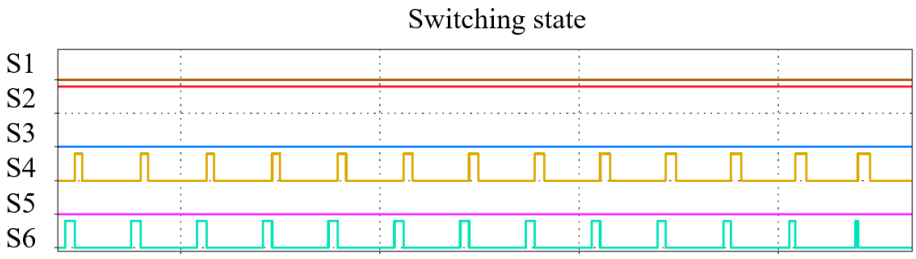

Figure 5-12 CSR FSM DCM detail

As shown in the figure above, during a switching period, there is one switch which is on all the time, and there are two other switches, one is turned on at the beginning of the switching period, and the other is turned on immediately after the other switch is turned off. Because of the fewer

device commutations, FSM has the advantages of less switching loss. Therefore, FSM is selected as the modulation approach for CSR in this work.

6 Simulation Study

In this thesis, the Matlab-Simulink and PLECS co-simulation models of 30 kVA Voltage Source Rectifier (VSR) and Current Source Rectifier (CSR) for 380VDC microgrid application is built. All the control functions are implemented in Simulink, and the electrical circuit is implemented in PLECS. This chapter documents the simulation model and its results. The simulation results of this chapter are employed to validate the analysis in Chapter 4.

6.1 Description of the Simulation Model

For the models of the VSR and CSR, the main components include the following:

- User Interface
- Controls
- Controls/VSR and Controls/CSR Interface
- Three-phase AC voltage source
- VSR or CSR circuit with DM CM filter and resistive load

And the following figures show the main components.

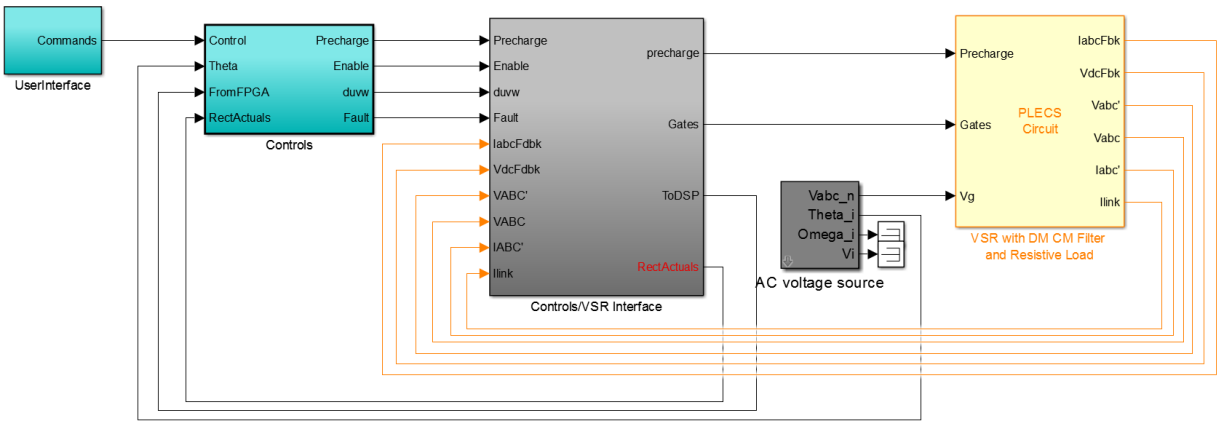

Figure 6-1 MATLAB-SIMULINK VSR simulation model (top level view)

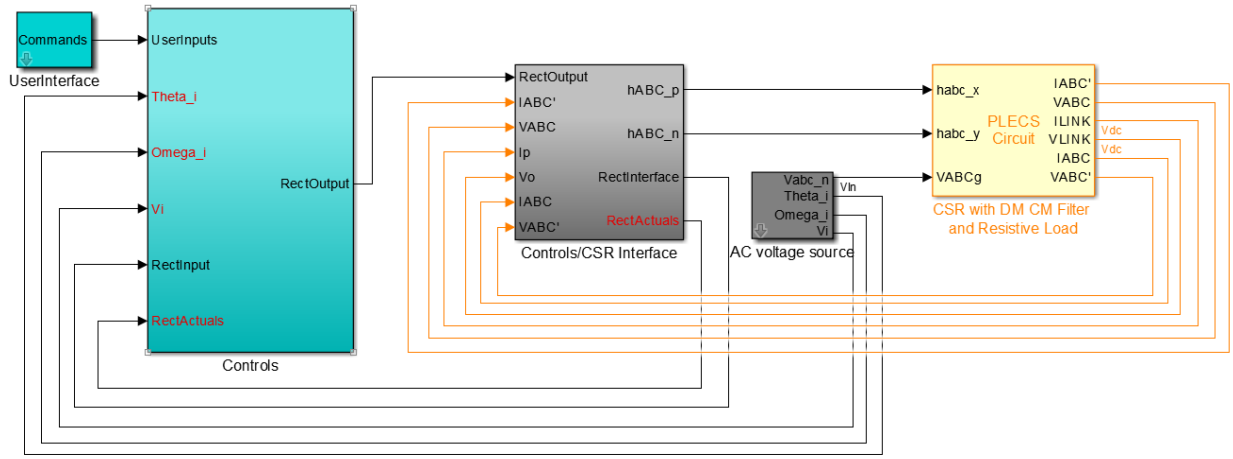

Figure 6-2 MATLAB-SIMULINK CSR simulation model (top level view)

The details of each component are given in following sub-sections.

6.1.1 Three-phase AC Voltage Source

The three-phase AC voltage source was used to provide amplitude and electrical position signals for the rectifier circuit implemented in the PLECS circuit. Also, it provides the instantaneous electrical angle and electrical angular frequency to CSR controller block.

6.1.2 VSR or CSR circuit with DM CM filter and resistive load

The VSR and CSR circuit with DM CM filter and resistive load are shown in Figure 6-3 and Figure 6-4. The signal of three controlled voltage sources comes from the three-phase AC voltage source Simulink block. Following figures show the VSR and CSR circuit simulation model with DM filter and CM filter correspondingly.

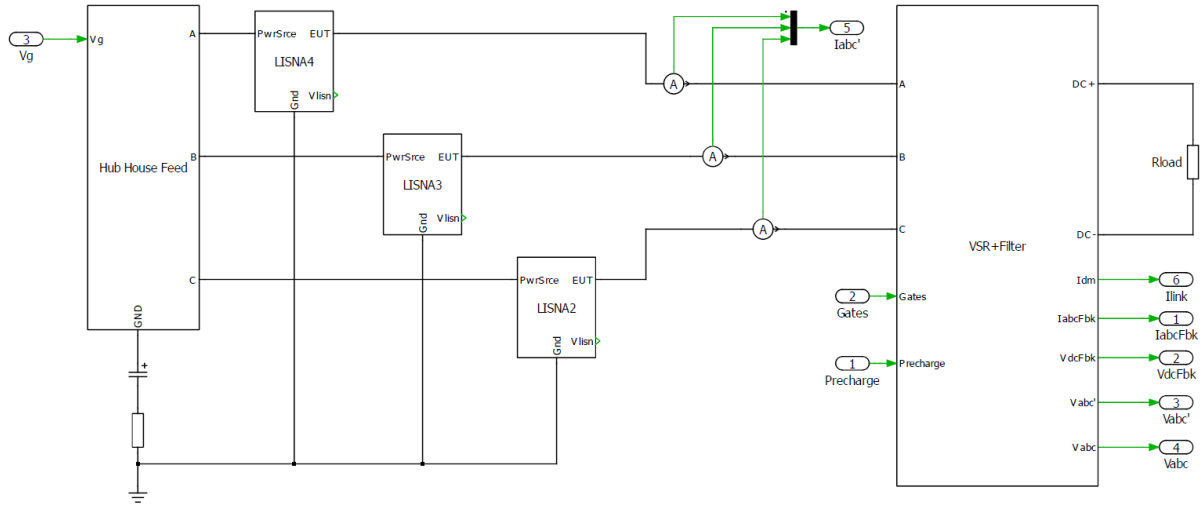

Figure 6-3 VSR circuit with DM CM filter and resistive load

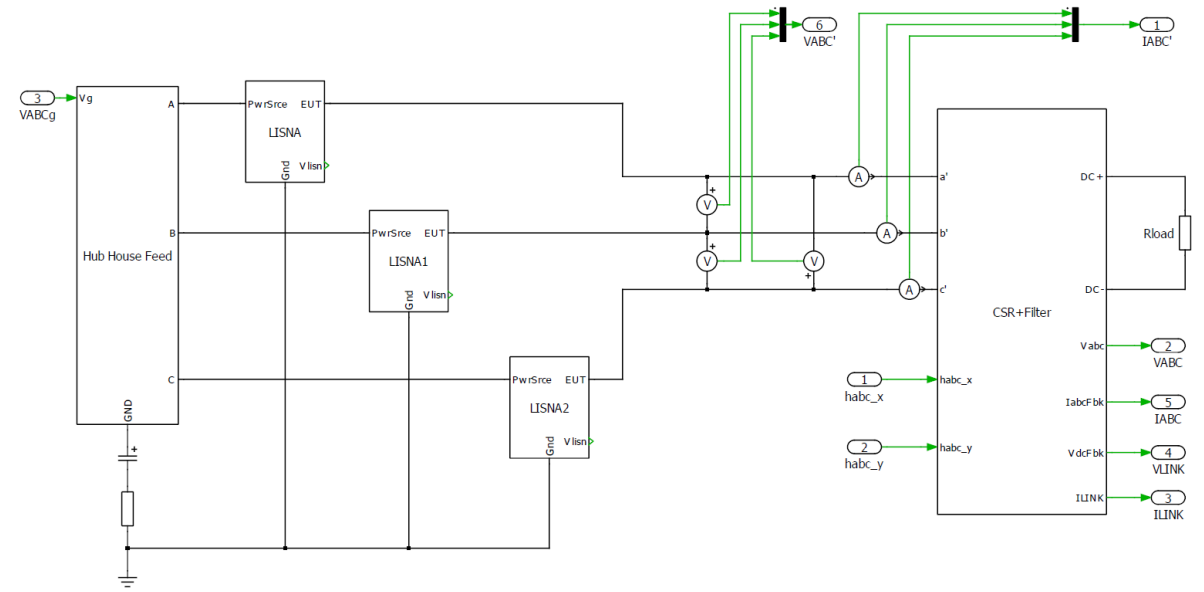

Figure 6-4 CSR circuit with DM CM filter and resistive load

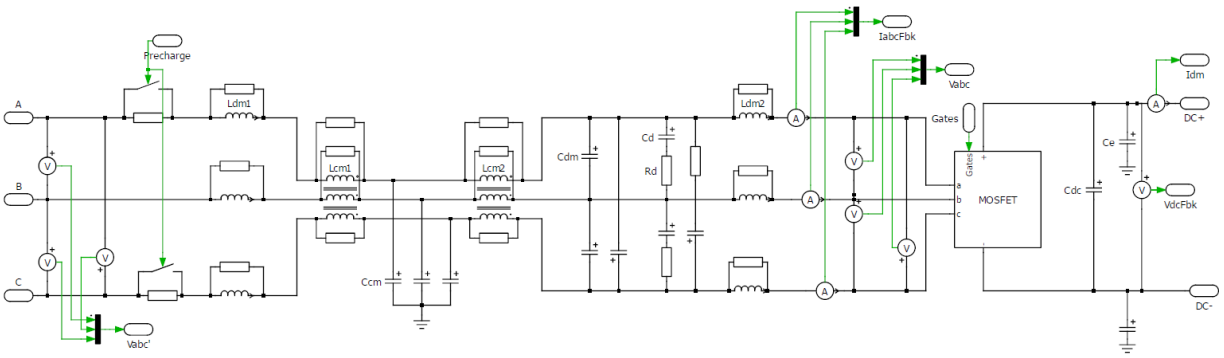

Figure 6-5 VSR circuit with DM CM filter

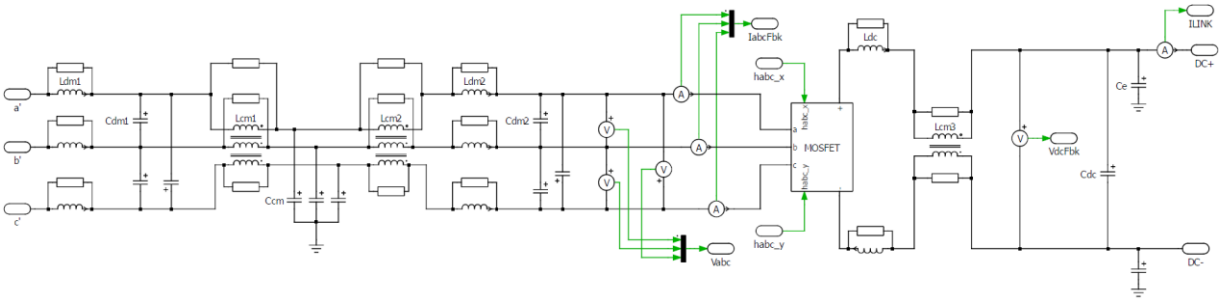

Figure 6-6 CSR circuit with DM CM filter

6.1.3 User Interface

The user interface contains the command input, including the start time, stop time, enable time, and so on. Following figures show the user interface of VSR and CSR.

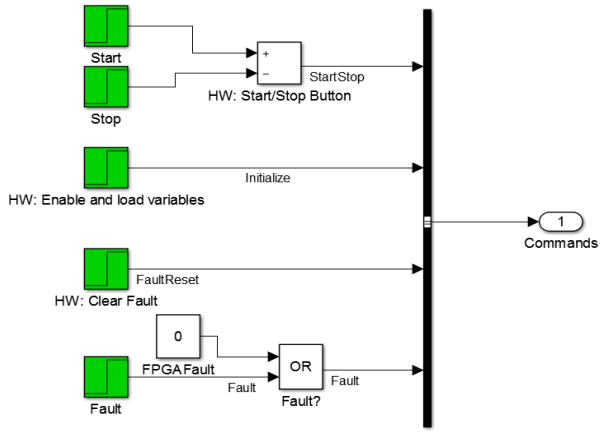

Figure 6-7 User interface of VSR

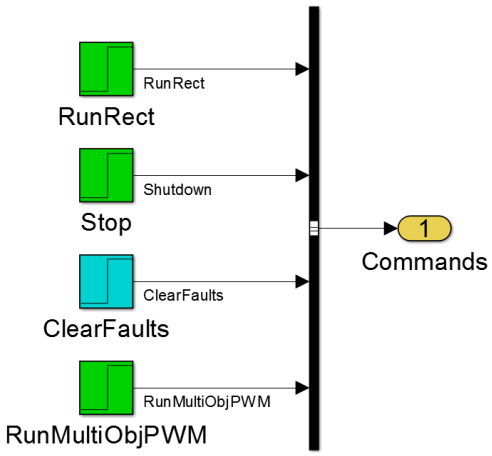

Figure 6-8 User interface of CSR

6.1.4 Controls/VSR and Controls/CSR Interface

The controls/VSR and Controls/CSR interface are put between controls and circuits, and its purpose is to condition the signals of the simulation and act as part of the hardware implementation, such as using an Anti-Aliasing filter (AAF) for filtering out noise above the Nyquist frequency.

6.1.5 Controls

Figure 6-9 shows the simulation blocks for the controls of VSR. The voltage controller ensures that the VSR output voltage V_{dc} tracks to the desired output voltage V_{dc}^*. The current in the dq0 frame is obtained by calculating the abc to dq0 transformation. The power factor is controlled by the value of i_q^*. The power factor can be regulated to zero by setting i_q^* to zero. The cross decoupling is employed to control the output voltage in the dq0 frame. Then by calculating the dq0 to abc transformation, the modulation index is obtained.

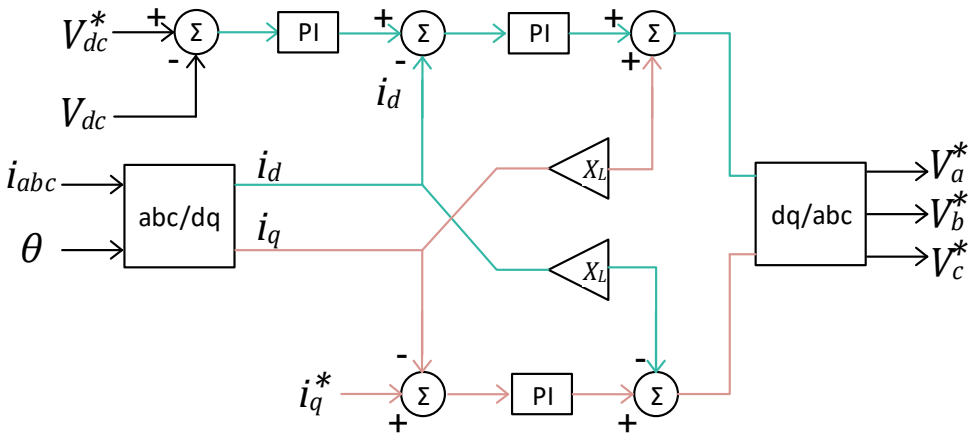

Figure 6-9 Voltage-Current controller implementation of VSR

Figure 6-10 shows the simulation blocks for the controls of CSR. The voltage controller ensures that the CSR output voltage V_{dc} tracks to the desired output voltage V_{dc}^*. And the cascaded

regulator for current is also employed to ensure that the dc-link current tracks to the desired current. The modulation index is obtained from the current PI regulator.

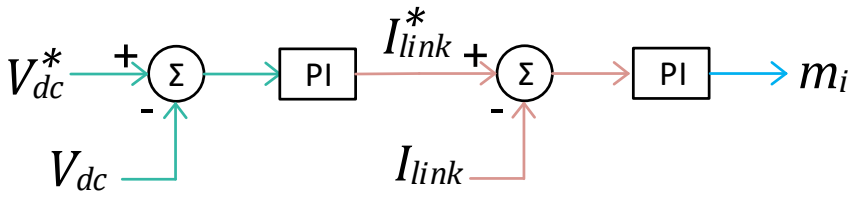

Figure 6-10 Voltage-Current controller implementation of CSR

6.2 Simulation Result

The filter has been designed, and the simulation model has been built with the DM and CM filter, and also the LISN is connected in the circuits, this section gives the simulation results measured from the model. By analyzing the measured current and voltage waveform, it is verified that the design of VSR and CSR meet the EMI standards, the noise has been significantly attenuated.

6.2.1 Voltage Source Rectifier Simulation Results

The spectrum of the measured LISN voltage measurement for the VSR is shown in Figure 6-11. The blue curve is the spectrum of the input current, the green curve is the spectrum of the LISN current, the red line is the IEC 61000-3-4 standards, the black line is the FCC 15 standards. This figure clearly shows that the spectrum meets the standards with the designed filters. Figure 6-12 gives the comparison of the input current and LISN voltage of VSR without and with a filter. It is obvious that there is lots of noise for the VSR without a filter, and the signal becomes much more sinusoidal with the design filter.

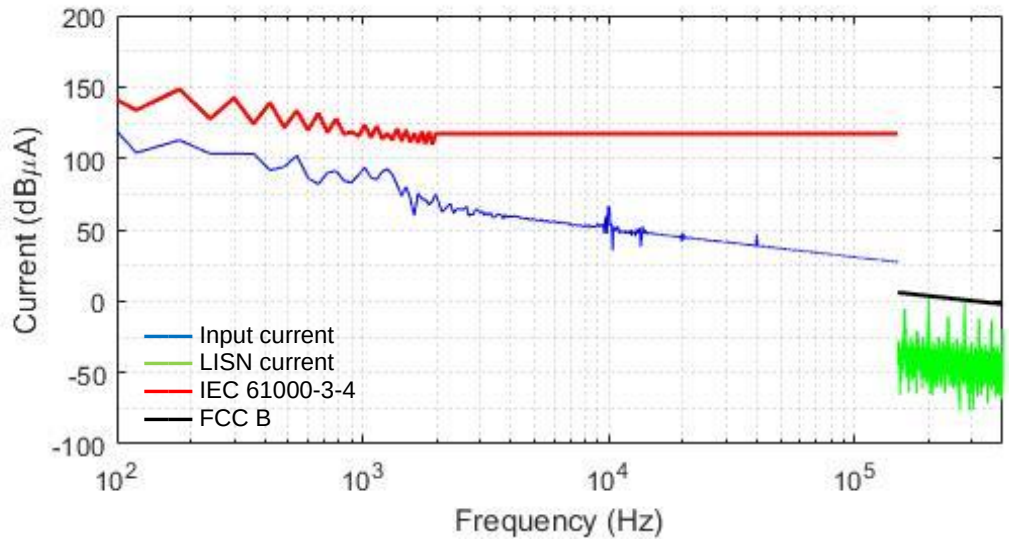

Figure 6-11 Spectrum of the input current and LISN current for the VSR

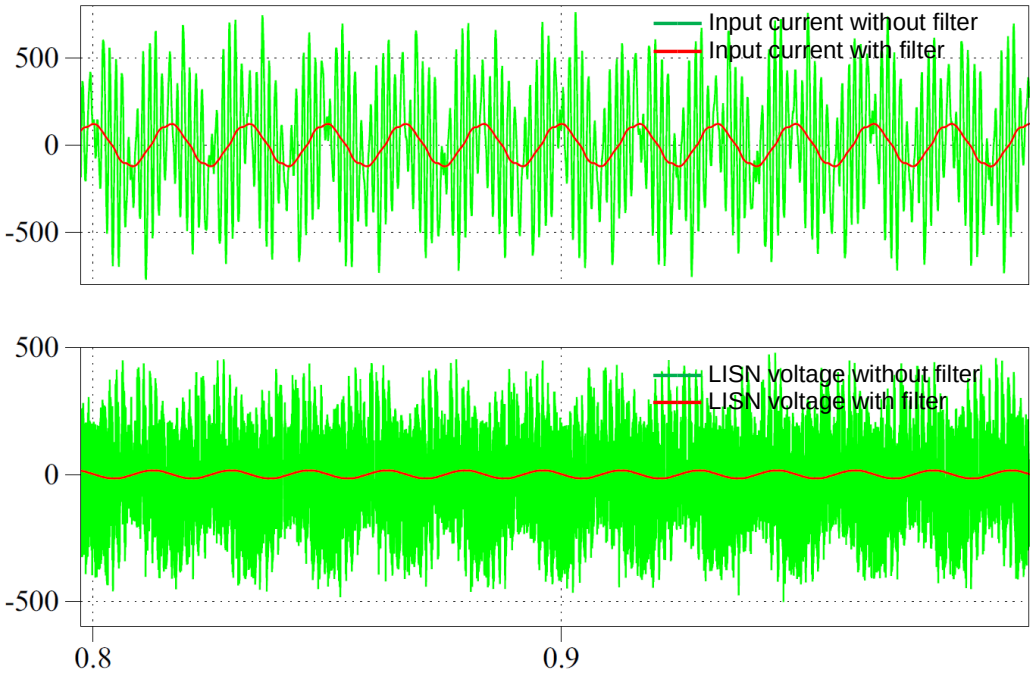

Figure 6-12 Input current and LISN voltage of the VSR

6.2.2 Current Source Rectifier Simulation Results

Figure 6-13 shows the spectrum of the measured LISN voltage measurement for the CSR. This figure clearly shows that the spectrum meets the standards with the designed filters. Figure 6-14

gives the comparison of the input current and LISN voltage of CSR without and with a filter. It is clearly that there is lots of noise for the CSR without a filter, and the signal becomes a much more sinusoidal wave with the designed filter.

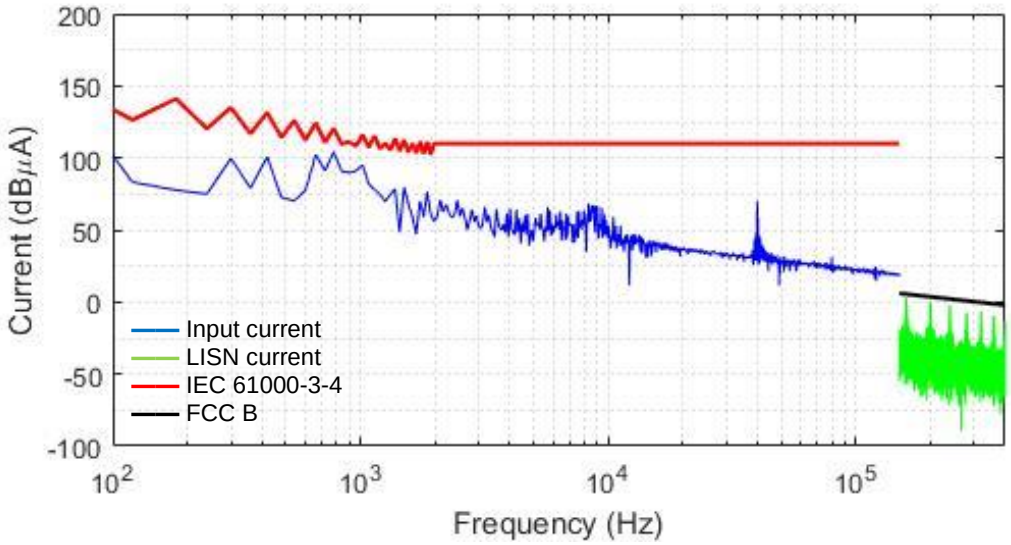

Figure 6-13 Spectrum of the input current and LISN current for the CSR

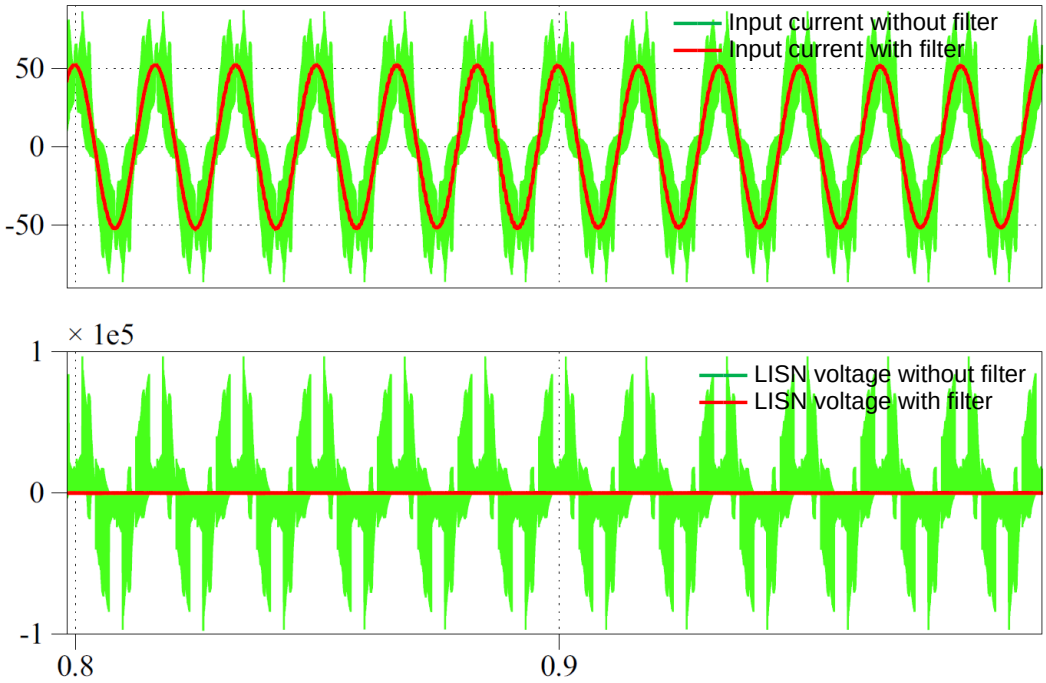

Figure 6-14 Input current and LISN voltage of the CSR

The selection of CM inductance is based upon a limitation of line to ground capacitance per each input phase to a value of C=0.5μF. The practice of limiting line to ground capacitance helps to control the level of circulating ground current in the system which is beneficial both from safety and CM filter design perspectives. This drives towards a larger common mode inductance which limits the flow of CM current—a consideration that is of particular relevance since the DC microgrid loads will include their EMI filters, with unspecified levels of capacitance to ground on the output. With a large CM inductor, the circulation of CM current between input and output of the active rectifier is kept to a low level. On the other hand, if a small CM inductance is selected with a high line to ground EMI filter capacitance, when the active rectifier is connected into the system, the resulting circulating current could cause the CM inductor to saturate. In this work, the total CM inductance values for VSR and CSR are 25.2 mH and 11.2 mH. According to [17] [18], the CM inductor parameters are selected for the calculation.

7 Experimental Setup

A generic three half-bridge is fabricated as a platform for experimental tests and it was used in [19] , [20]. Mitigation of parasitic capacitances and inductances within the test fixture was a major objective in designing the LISNs. The high-frequency behaviors of the VSR and CSR implementations will be characterized utilizing the test platform. The hardware for the VSR has already been designed and constructed with particular consideration for mitigating high-frequency DM and CM resonances and superior performance on one half-bridge has been validated [19] , [20]. This minimization of the gate drive and bus layout interconnection and cross-coupling inductances were considered in developing the platform. Three half-bridge power modules are mounted on a common printed circuit board (PCB) and design of the PCB is a multi-layer interleaved design. Each half-bridge power module is controlled by an independent gate driver which consists of two isolated gate driver channels for driving the high-side and low-side devices, respectively. The gate driver design is comprised of a high-bandwidth magnetically isolated signal interface, a commercially available gate drive integrated circuit, and a high-current BJT totem pole output stage. The size of the designed power electronic hardware was used in developing the developing the power density estimates. Figure 7-1 shows the developed platform for the experimental tests.

The LISN was designed to tolerate unfiltered switching pulses and high dv/dt contributions. LISN inductors were designed to withstand the rated currents while minimizing inter-winding capacitance and having linear inductance to high frequencies for instance 10MHz. LISN inductors were placed far from the rest of the system to minimize the possible electromagnetic coupling. Figure 7-2 shows the developed LISN. Future work will utilize measured data from the test fixture

and the design process outlined in this paper to design optimal filters for the VSR implementation. This work will be followed by similar design of the CSR. Actual hardware characterizations will enable consideration of the design beyond the 400kHz frequency range. High-frequency considerations of the inductor designs must also be taken into account.

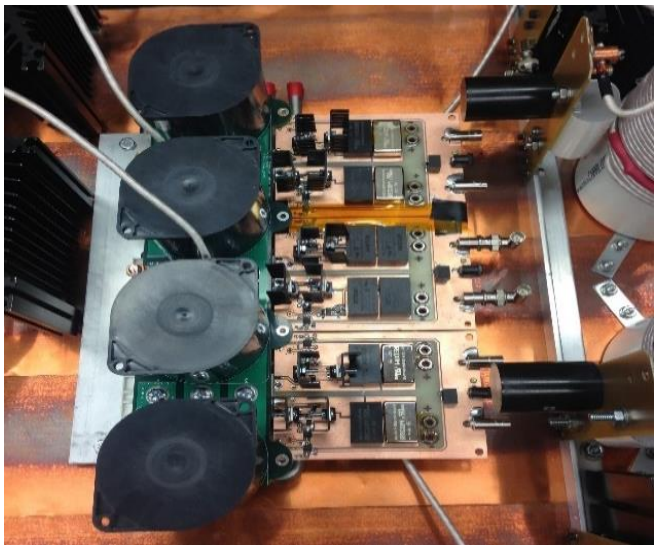

Figure 7-1 Three phase platform with three independent gate drivers

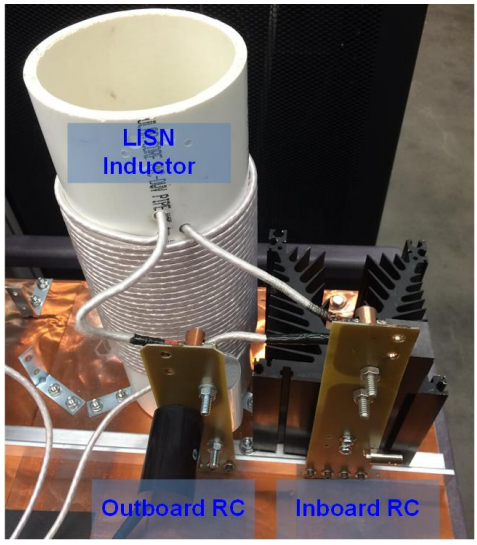

Figure 7-2 Developed LISN

8 Conclusion and Future Work

8.1 Conclusion

VSR and CSR were designed using SiC half bridge module for applications in community DC microgrid. Appropriate filters were designed to meet the required harmonics and EMI standard limits. The comparison of the calculated efficiency and power density of the rectifiers indicate that both higher power density and efficiency is achieved with the CSR system for the specific 350Vdc microgrid application. The most significant reason for the power density and subsequent efficiency improvement is that the CSR enables placement of filter components in places where the high-frequency stresses imposed by the switching power converter have less impact. Essentially, the CSR contains the pulsed switching frequency behavior on the AC side within its circuit structure while the VSR applies both CM and DM pulsed voltages to the AC system that must be absorbed by the closest inductors in the filter structure. This work indicates, finally, that the CSR is not only a good choice for the interface between the AC and DC systems from the standpoint of fault mitigation but also from the standpoint of EMC.

8.2 Future Work

It is recognized that the CSR carries the penalty of only unidirectional power flow, which is a major limitation to the DC microgrid implementation, this aspect of the system design can be improved. Also, the EMI inductor design and material selection need further explorations to achieve the lower loss and smaller volume. Finally, the wide band gap device results in the challenge of high-frequency effects even in the microwave electronics domain; this is an additional and significant area for future work.

References

[1] R. Cuzner, K. Palaniappan and J. Shen, "System Specification for a DC Community microgrid and living laboratory embeded in an Urban Environment," *IEEE, ICRERA*, pp. 1119 - 1125, 2015.

[2] Department of Energy Office of Electricity Delivery and Energy Reliability, "Summary Repart: 2012 DOE Microgrid workshop".

[3] N. Mohan, T. Udeland, and W. Robbins, Power Electronics: Converters, Applications and Design, 2nd ed, New York: Wiley, 1995.

[4] Cree, "1200V, 100A, Silicon-Carbide Half-Bridge Module, CAS100H12AM1 datasheet," 2012.

[5] T. Nussbaumer, M. Baumann, and J. W. Kolar, "Comprehensive design of a three-phase three-switch buck-type PWM rectifier," *IEEE Trans. on Power Electronics*, Vols. 22, no. 2, pp. 551-562, Mar. 2007.

[6] R. Cuzner, D. Drews, G. Venkataramanan, "Power Density and Efficiency Comparisons of System-Compatible Drive Topologies," *Industry Applications, IEEE Transactions*, Vols. 51, no.1, pp. 459-469, Jan.-Feb. 2015.

[7] J. He, T. Zhao, X. Jing, and N. A.O. Demerdash, "Application of Wide Bandgap Devices in Renewable Energy Systems – Benefits and Challenges," *3rd International Conference on Renewable Energy Research and Applications*, 2014.

[8] N. Pasi, P. Antti, S. Juha-P, K. Tero, and S. Pertti, "On Common-Mode and RF EMI in a Low-Voltage DC Distribution Network," *IEEE Transaction on Smart Grid*, Vols. 5, no. 5, sep. 2014.

[9] W. Fu, Q. Jiao, R. Hosseini and R. Cuzner, "Methodology for the volume minimization in non-isolated SiC based PV inverters," *IEEE ICRERA*, pp. 1236-1242, 2015.

[10] A. Nagel and R. W. De Doncker, "Systematic design of EMI-filters for power converters," *in Conf. Rec. IEEE IAS Annu. Meeting*, vol. 4, p. 2523–2525, Oct. 2000.

[11] T. Nussbaumer, M. L. Heldwein, and J. W. Kolar, "Differential mode input filter design for a three-phase buck-type PWM rectifier based on modeling of the EMC test receiver," *IEEE Trans. Ind. Electron.*, Vols. 53, no. 5, p. 1649–1661, Oct. 2006.

[12] A. D. Brovont; S. D. Pekarek, "Derivation and Application of Equivalent Circuits to Model Common-Mode Current in Microgrids," *in IEEE Journal of Emerging and Selected Topics in Power Electronics*, Vols. PP, no.99, pp. 1-1, 2016.

[13] A. D. Brovont and S. D. Pekarek, "Equivalent circuits for common-mode analysis of naval power systems," *2015 IEEE Electric Ship Technologies Symposium (ESTS),* pp. 245-250, 2015.

[14] J. Li, T. Abdallah, and C. Sullivan, "Improved Calculation of Core Loss with Nonsinusoidal Waveforms," *IAS 2001*.

[15] Q. Jiao, R. Hosseini and R. Cuzner, "A Comparison between Silicon Carbide Based Current Source Rectifier and Voltage Source Rectifier for Applications in Community DC Microgrid," *2016 International Conference on Renewable Energy Research and Applications (ICRERA),* submitted for publication, November 2016.

[16] T. Halkosaari and H. Tuusa, "Optimal vector modulation of a PWM current source converter according to minimal switching losses," *IEEE 31st Annual Power Electronics Specialists Conference,* vol. 1, pp. 127-132, 2000.

[17] S. D. Sudhoff, G. M. Shane and H. Suryanarayana, "Magnetic-Equivalent-Circuit-Based Scaling Laws for Low-Frequency Magnetic Devices," *IEEE Transactions on Energy Conversion,* vol. 28, pp. 746-755, Sept. 2013.

[18] R. Zowarka, "Physical scale modeling to verify energy storage inductor parameters," *IEEE Transactions on Magnetics,* vol. 20, pp. 219-222, Mar 1984.

[19] A. Lemmon, R. Graves, and J. Gafford, "Evaluation of 1.2 kV, 100A SiC Modules for High-Frequency, High-Temperature Applications," *Applied Power Electronics Conference and Exposition (APEC),* pp. 789-793, 2015.

[20] R. Cuzner, R. Hosseini, A. Lemmon, J. Gafford, M. Mazzola, "Control and Characterization of Electromagnetic Emissions in Wide Band Gap Based Converter Modules for Ungrounded Grid-Forming Applications," *IEEE Applied Power Electronics Conference* , pp. 1577-1584, 2016.

[21] A. Nagel and R. W. De Doncker, "Systematic design of EMI-filters for power converters," *in Conf. Rec. IEEE IAS Annu. Meeting,* vol. 4, p. 2523–2525, Oct. 2000.

[22] R. Cuzner,A. Esmaili, "Fault tolerant shipboard MVDC architectures," *International Conference on Electrical Systems for Aircraft, Railway, Ship Propulsion and Road Vehicles, 2015 IEEE (ESARS),* March 3-5, 2015.

[23] R. Cuzner, V. Singh, M. Rashidi, A. Nasiri, "Converter topological and solid state protective device trade-offs for future shipboard MVDC systems," *IEEE , ICRERA,* pp. 34-39, 2015.

[24] C. P. Steinmetz, "On the law of hysteresis," Proc IEEE, 1984, pp. 196-221, 2.